Thesis for the Degree of Master

Fabrication of Thiol-norbornene Photo-crosslinked Pectin Nanogels for Transcutaneous Immunization

경피면역요법을 위한 티올-노보닌 광가교 펙틴 나노젤의 제조

August 2021

Siyeong Lee

Department of Agriculture, Forestry and Biosources

SEOUL NATIONAL UNIVERSITY

Fabrication of Thiol-norbornene Photo-crosslinked Pectin Nanogels for Transcutaneous Immunization

경피면역요법을 위한 티올-노보닌 광가교 펙틴 나노젤의 제조

지도 교수 기 창 석

이 논문을 농학석사 학위논문으로 제출함
2021년 6월

서울대학교 대학원
농림생물자원학부 바이오소재공학 전공
이 시 영

이시영의 농학석사 학위논문을 인준함
2021년 8월

위 원 장 _____ 김 태 일
부위원장 _____ 기 창 석
위 원 _____ 곽 선 영

Abstract

Transcutaneous immunization (TCI) delivers antigens directly to immune cells of the skin and inoculation is non-invasive. In general, a specific antigen may target Langerhans cells (LCs) or dermal dendritic cells (DCs), bypassing metabolic degradation. However, it is difficult to deliver antigens to immune cells due to the skin barrier. A novel transcutaneous antigen delivery carrier was developed using pectin from citrus peel. This biocompatible and immunoactive biopolymer was functionalized with norbornene groups creating a hydrogel network for thiol-ene photo-click reaction with dithiol crosslinkers and ovalbumin (OVA). A pectin nanogel was formed by facile sonication; the particles were of uniform size (~200 nm in diameter). In porcine skin penetration tests, pectin nanogels penetrated the stratum corneum and were deposited in the epidermis and dermis. The nanogels were then internalized by dendritic cells derived from THP-1 monocytes, inducing cell maturation. Thus, pectin nanogels will find applications in transcutaneous antigen delivery.

Keyword: Transcutaneous immunization, Pectin, Photo-click chemistry, Nanogels, Dendritic cells

Student Number: 2019-21536

Table of Contents

List of Tables

List of Figures

I. INTRODUCTION

Immunomodulation, a form of immunotherapy, aims to regulate the immune response by either stimulating or suppressing immune activity [1-3]. Generally, immunomodulation is achieved by delivering immunomodulators or antigens to immune cells such as T-cells, macrophages, and dendritic cells (DCs) [3, 4]. In particular, DC plays an important role in adaptive immunity as an antigen presenting cell, activating other immune cells. Various methods delivering immunomodulators or antigens to dendritic cells have been extensively studied to improve delivering efficiency. Transcutaneous immunization (TCI) is a convenient and non-invasive antigen delivery method by passing the first-metabolism or by avoiding early degradation in gastrointestinal tract [5]. TCI could directly target various immune cells (e.g., Langerhans cells [LCs], dermal DCs, dermal T-cells) in skin [5, 6].

However, delivery is challenging because the skin is a natural barrier. The stratum corneum (SC), a hydrophobic top layer of dead cells, has tightly packed corneocytes, lipids, and extracellular matrix (ECM) proteins [5, 7]. Such an integrated structure does not allow the penetration of large molecules such as protein or polysaccharide-based antigens. To achieve the dermatological antigen delivery, nanoparticles have been explored as a carrier. However, several nanoparticles including liposomes, transferosomes, and solid lipid nanoparticles (SLN) have also limitation due to low drug loading efficiency [8-10].

A nanogel is a three-dimensional, highly crosslinked nano-sized hydrogel network recently used to deliver dermatological antigens [11]. The network readily accepts various functional groups and polymers, and thus has excellent versatility and allows programmed release of loaded antigens. Nanogels can either entrap antigens for later release or immobilize them using various functional groups of the backbone polymer. Thus, controlled antigen or drug release is possible. However, nanogel-based dermatological antigen delivery is compromised by low SC permeability compared to that of lipid-based nanoparticles [11]. In the past decade, hyaluronic acid (HA)-mediated transdermal delivery has been reported [12-14]. It is assumed that its amphiphilicity and skin hydration enables skin penetration.

Pectin, a natural biopolymer of plant cell walls, is biocompatible and safe, and widely utilized in the food, cosmetic, and pharmaceutical industries as a thickener and coating agent [15]. It is a polymer of 1,4-α-D-galacturonic acid that is partially methyl- or acetyl-esterified, and is amphiphilic in nature [16]. Furthermore, pectin is recognized by pattern recognition receptors (PRRs) such as Toll-like receptors (TLRs) on the surface and endosomes of various phagocytes (e.g., DCs and macrophages), resulting in internalization and cell activation [17-19].

Thus, the structural similarities between pectin and HA, and the effect of pectin on phagocytes are thought to be able to solve above problems. To create a skin delivery carrier, we synthesized pectin-norbornene (pectin-NB)

derivatives via photo-click crosslinking and incorporated a model antigen (OVA). Through simple ultrasonication, the pectin hydrogel was reduced to nanogels. The procedure was optimized and skin permeability of nanogels were defined using porcine skin in vitro. Then nanogel internalization was examined by DCs derived from a monocytic leukemia cell line (THP-1), and the resulting effects on the immune system.

II. LITERATURE SURVEY

Immunotherapy is the approach to treating diseases by inducing an immune response to it [20]. As part of immunotherapy, immunomodulation is commonly administrated as injections to stimulate specific immune response [21]. It induces immunologic memory against subsequent infections. Though classic vaccination administered as injections are effective in causing desired immune response, it has several disadvantages such as needle-related pain, injuries or poor patient compliance [22-24]. The reuse of needles also causes a severe problem of high mortality [23]. Therefore, the immunomodulation method without needle injection can be free from the problems.

Transcutaneous immunization (TCI) involves topical application of antigens or immunomodulators to the epidermis [5,6,21]. TCI targets the active immune-related agents of the skin to induce functional immune responses [5]. It is non-invasive and painless method so that easily applied to children and the elderly. Also, TCI is convenient because it can reduce clinical setting or medical supervision for self-administration capability [24]. Antigen delivery through TCI is efficient as there is no first-pass liver metabolism or gastrointestinal tract degradation [25]. Several cases of TCI using protein or DNA antigen have been reported [21,24]. Thus, it could be an alternative vaccination route against injection that infection and needle phobia do not need to be considered.

TCI is attractive because the skin area is large, and the skin contains numerous T-cells, macrophages and DCs. The latter play an important role in adaptive immunity. DCs are antigen-presenting cells that activate other immune cells [26,27]. DCs recognize and capture invading antigens and present them to other immune cells when draining lymph nodes. Especially, T-cell is stimulated and activated by antigen presentation of DCs [28]. The antigen is presented by the DC matured from the immature state, which then activates the T cell. Dermal DCs are generally more mobile than other immune cells lying beneath the skin such as LCs [5,29]. Because of these reasons, various methods have been used to deliver immunomodulators and antigens to skin DCs [3,5,6].

However, it is challenging for antigens to be delivered underneath skin layers due to the barrier property of Stratum Corneum (SC) [1,3-5,30]. The SC structure is “bricks-and-mortar”-like; the bricks are keratinocytes and the mortar is the surrounding lipid matrix. Because this SC structure acts as a barrier to protect the skin from the outside, the entry of foreign substances is difficult. Dermal delivery is constrained by the “principle of 500 Daltons”; particles larger than 500 Da cannot penetrate the skin barrier [31,32]. Under the SC, the epidermis has densely packed keratinocytes and a basement membrane, and is thus also impregnable to large molecules such as protein- and polysaccharide-based antigens [2,6,7,31]. Though it is easier to penetrate SC for highly lipophilic or small molecules, skin layers hardly pass other compounds.

Therefore, to achieve a successful immunization crossing the SC and reaching immune cells for antigen presentation, various methods have been suggested [5,33]. The first method is to use chemical enhancers such as ethanol, methanol, and glycols. These enhancers disrupt the SC and improve the skin penetration ability of the compound. The second is a physical enhancement method such as iontophoresis, microneedles, and sonophoresis. This method allows antigen to bypass the SC and penetrate into the skin [7,13].

However, by using a nanoparticle-type carrier, it is possible to increase the skin transmittance without greatly receiving the help of enhancement. Nanoparticles have been used to deliver dermatological antigens overcoming SC [33]. Liposomes are spheres composed of cholesterol/phospholipid bilayers; they are biodegradable, non-toxic, and capable of hosting both hydrophilic and hydrophobic substances [33,34]. Because they are lipophilic, it is advantageous for storing substances with good skin penetration and low solubility. However, liposomes are large and lack elasticity [9]. Also liposomes are vulnerable to external deformation or decompositions. Transferosomes, which are highly elastic and deformable, exhibited better skin penetration [30,33]. Transferosomes are liquid-state vesicles composed of phospholipids with an edge activator. They squeeze and penetrate into SC under the influence of a water gradient and are deposited in the subcutaneous tissue. However, they are ineffective at delivering hydrophobic drugs [8]. Lipid nanoparticles can serve as colloidal carriers; they allow long-term drug release, are physically stable, and prevent drug

degradation. Solid lipid nanoparticles (SLNs), which are colloidal and highly flexible, afforded stable, long-term hydrophobic drug release. However, drug loading efficiency was relatively low. There is a possibility of drug release from SLN during storage. [9,33,35].

Nanogels are highly crosslinked nano-sized hydrogels of three-dimensional network structure recently highlighted as topical antigen delivery carriers [11,36,37]. Generally, the size of nanogels ranges from 10-200 nm, known to be suitable for dermal penetration. The hydrophilic polymers of the network are compatible with those of common antigens (e.g., proteins) [38,39]. Recently, photo-click hydrogel crosslinking has been used to create well-defined networks varying in hydrogel properties and drug-loading efficiency [12,40]. Nanogels have been used to deliver topical antigens [11]. The particle size ranges from 10–200 nm, permitting dermal penetration. Nanogels entrap hydrophilic antigens and other molecules (e.g., proteins or peptides). Unlike conventional nanocarriers, there are no restrictions on the types of drugs that can be loaded [11,39]. Son et al. fabricated hyaluronic acid (HA)-based nanogels that incorporated lipophilic drugs during self-assembly. The nanogels penetrated the SC and delivered drugs to the epidermis and dermis [25]. Toyoda et al. created polyethylene glycol-based nanogels hosting antigenic peptides. The nanogels penetrated the SC and delivered peptides to resident LCs, thereby reducing tumor volume [36].

HA is a natural polysaccharide composed of repeating unit of D-glucuronic acid and N-acetyl-D-glucosamine linked with altering β-1,4 and β-1,3 glycosidic bonds [12,41]. It is widely used in biomedical fields for its biocompatibility. Especially, HA penetrate skin despite its hydrophilicity and large molecular size. Although the mechanism remains unclear, it is suggested that the amphiphilicity of HA, and keratin hydration thereof, are important [41,42]. Kim et al. conjugated ovalbumin (OVA) to HA; the nanocarrier enabled transdermal vaccination, penetrating the skin followed by DC internalization and activation [13]. Kim et al. prepared a crosslinked HA nanogel conjugated with beta-glucan, which was internalized by DCs and then triggered DC maturation. HA-antigen conjugates and HA/β-glucan hybrid nanogels were used to target dermal phagocytes [12]. Despite these advantages, there is a problem with the use of HA as a transdermal antigen delivery carrier. High molecular weight HA interferes with receptor-mediated internalization on the cell surface [42]. This can interfere with the uptake of antigens by dendritic cells after skin penetration, which can be an obstacle to inducing immunity.

Pectin is a natural biopolymer comprising plant cell walls that surround growing cells. It is well known to have biocompatibility and biological safety [15, 42]. Due to these features, pectin is widely utilized in food, cosmetic, and pharmaceutical industries as a thickener, stabilizing or coating agents [16]. Pectin has linear homogalacturonan (HG) domains and “hairy” rhamnogalacturonan (RG) domains. In general, HG is the major

component of pectin composed of 1,4-α-D-galacturonic acid with partially methyl-esterified or acetyl-esterified branches. Through hydrophilic backbone and hydrophobic groups, pectin is thought to have amphiphilic properties [16,43,44].

Meanwhile, recent studies revealed the bioactivity of pectin. There are a number of studies on the effect of pectin in reducing tumor metastasis [18,44,45]. Pectin modified by pH or heat may induce apoptosis of cancer cells or may exhibit antitumor activity. In addition, pectin has been shown to exert immune effects via interaction with pattern recognition receptors (PRR) such as toll-like receptors (TLR). TLR is presented in cell surface or endosome membranes of various phagocytes (e.g., DC and macrophage) [46,47]. Pectin interacts with PRR depending on its chemical structure. Recent studies have shown that cell membrane TLR-2 and 4 or endosome membrane TLR-9 may be involved in cell internalization of pectin [17-19,48]. Therefore, pectin is expected to be recognized and incorporated into cells and activate immune cells.

III. MATERIALS AND METHODS

3.1. Materials

5-norbornene-2-methylamine (≥ 98%) was purchased from Tokyo Chemical Industry (Tokyo, Japan). 4-morpholineethanesulfonic acid monohydrate (MES hydrate, 98%) was from Alfa Aesar (Haverhill, MA, USA). 1-(3-dimethylaminopropyl)-3-ethylcarbodiimide hydrochloride (EDC, ≥ 98%) was purchased from Acros Organics (Geel, Belgium). Ethylenediaminetetraacetic acid (EDTA, ≥ 98%) was from Daejung (Siheung, Korea). All other chemicals, including pectin from citrus peel and lithium phenyl-2,4,6-trimethylbenzoylphosphinate (LAP, ≥ 95%), were purchased from Sigma-Aldrich (St. Louis, MO, USA) unless otherwise indicated.

3.2. Synthesis and characterization

To synthesize pectin-NB, intact pectin was dissolved in MES buffer (0.1 M, pH 6) at 16 mg/mL. To activate the carboxyl groups of pectin, one molar equivalent of EDC was added per galacturonic acid unit of pectin, followed by stirring for 1 h at 25 ºC. Then, 5-norbornene-2-methylamine (at molar ratios of 1, 2, or 4) was added, and the pH was adjusted to 5–6. Each mixture was held for 24 h in the dark, followed by addition to cellulose acetate tubes (molecular weight cutoff = 12–14 kDa), dialysis against deionized water for 3 days, and lyophilization.

To synthesize thiolated OVA (OVA-SH), OVA (≥ 98%) was dissolved in phosphate-buffered saline (PBS) with 2 mM EDTA at 10 mg/mL, and the pH was adjusted to 8. Traut's reagent (≥ 98%) was also dissolved in PBS to 14 mM, and 33.43 μL was added to the OVA solution; the Traut's reagent was thus in a 2-fold molar excess. The mixture was stirred for 1 h at room temperature, dialyzed, and lyophilized.

Rhodamine B-labeling of OVA-SH (OVA-SH-Rho) was synthesized as described previously [49]. Briefly, lyophilized OVA-SH powder (300 mg) was dissolved in 15 mL of sodium carbonate buffer (0.1 M, pH 9.2). Rhodamine B isothiocyanate (3 mg, at 2.5 mg/mL in dimethyl sulfoxide [DMSO]) was added to the OVA-SH solution and the mixture was stirred for 1 h at room temperature. Unreacted rhodamine B isocyanate was quenched by addition of Tris buffer (≥ 99.8%, 1.0 M, pH 8.3; Bio-Rad, Hercules, CA, USA) for 30 min. The reaction mixture was dialyzed in the dark and lyophilized. The extent of norbornene (NB) modification was determined by proton nuclear magnetic resonance (^{1}H-NMR) spectroscopy (600 MHz; Bruker, Billerica, MA, USA).

3.3. Bulk hydrogel fabrication

Pectin-NB was dissolved in PBS (pH 7.4), with dithiothreitol (DTT, ≥ 97%) used as a crosslinker and LAP as a photoinitiator. The concentration of pectin-NB in the prepolymer solution was 0.5–2.0% and the DTT concentration was 1.25–6.5 mM. OVA-SH or OVA-SH-Rho was added to various concentrations (0.1–0.4 mM). The LAP concentration was fixed at 1 mM in all cases. The precursor solution (two aliquots of 65 μL) were injected into two glass slides separated by 1 mm-thick spacers, followed by ultraviolet (UV) irradiation (10 mW/cm^2, 365 nm) for 2 min. The gel fraction was determined by measuring the weight of dried hydrogel (W_{dried}) after washing in deionized water for 24 h at 37 ºC, which removed soluble materials:

$$\text{Gel fraction (\%)} = W_{dried}/W_{theoretical} \times 100 \quad (1)$$

where $W_{theoretical}$ is the combined weight of the initially added network components. The mass swelling ratio (q) was measured after 24 h incubation in PBS at 37 ºC as follows:

$$q = W_{swollen}/W_{dried} \quad (2)$$

where $W_{swollen}$ was the weight of the swollen hydrogel measured after removal of excess PBS using wipes.

3.4. Rheometry

To measure shear moduli, hydrogels were incubated in PBS for 24 h and circular discs (diameter = 8 mm) were punched out using a biopsy punch. Gel moduli were measured using an 8-mm parallel plate with a nominal force of 0.2–0.3 N and a gap of 0.85 mm. The average G′ value for each sample was obtained in the linear viscoelastic region (LVR). The crosslinking density (ν) was calculated as:

$$G' = \nu RT \quad (3)$$

where G′, R, and T are the shear storage modulus, gas constant, and temperature (K), respectively.

3.5. Nanogel fabrication

Pectin-NB nanogels fabrication was performed according to a previously established protocol [12]. Briefly, one hundred-microliter volumes of prepolymer solution were subjected to UV light-emitting diode (UV-LED) spot curing (SP-LED-1; Ushio, Tokyo, Japan) at 10 mW/cm^2 for 2 min with vortexing. Photopolymerized gels were then dispersed in 400-μL amounts of PBS, followed by ultrasonication at various powers (26–104 W) for various times (30–120 s) using a tip sonicator (VCX-130; Sonics & Materials Inc., Newtown, CT, USA). The nanogels were centrifuged, washed with PBS, and filtered through 0.45-μm pore-sized syringe filters.

3.6. Nanogel characterization

Nanogels were dispersed in 1-mL amounts of PBS and subjected to dynamic light scattering (DLS) evaluation using a Zetasizer Nano ZS90 (Malvern Panalytical, Malvern, UK) operating at 633 nm and 25 ºC with a 90° detection angle. Particle sizes, stabilities, and distributions were evaluated using a nanoparticle tracking analyzer (Nanosight LM10; Malvern Panalytical) equipped with a 640-nm laser. To evaluate stability, nanogels at various concentrations were incubated in PBS at 4, 25, and 32 ºC for 8 days. Nanogel size was measured using the Zetasizer after nanogel pelleting and resuspension at each time point. To evaluate degradation, nanogels of various concentrations were incubated in PBS at 32 ºC with 10 mg/mL lysozyme (≥ 90%).

The nanogels were placed on grids (Quantifoil R1.2/1.3, 200 mesh; Electron Microscopy Sciences, Hatfield, PA, USA) cleaned by glow discharge (PELCO easiGlow; Ted Pella, Redding, CA, USA). Each sample was blotted for 1.5 s at 100% relative humidity and 4 ºC, and vitrified in liquid ethane using a plunge-freezing system (Vitrobot Mark IV; Thermo Fisher Scientific, Waltham, MA, USA). The frozen nanogels were observed under a transmission electron microscope (Talos L120C; Thermo Fisher Scientific) operating at an acceleration voltage of 120 kV.

3.7. Skin penetration

Intact porcine skin was obtained from a local market immediately after sacrifice and stored at –80 ºC. Skin specimens with an electrical resistance of 0.5–0.7 kΩ were used in all experiments [7,13]. Prior to testing, frozen skin was conditioned at 32 ºC for 10 min, gently washed with PBS, briefly dried, cut into 2 × 2 cm pieces and placed in Franz diffusion cells (model 4G-01-00-11.28-08; PermeGear, Hellertown, PA, USA). The recipient chamber was filled with PBS and maintained at 32 ºC by passing warm water through the jacket. One-hundred-microliter amounts of OVA-rhodamine B solution and rhodamine B-labeled nanogels (4×10^8 nanoparticles/mL) were applied to the skin surface via the donor chamber. The OVA levels were identical between the OVA solution and nanogel. After 24 h, the skin samples were fixed in 4% (v/v) formaldehyde, washed, embedded in cutting compound at –80 ºC, and cryo-sectioned (10-μm-thick slices) using a cryo-microtome (CM1850; Leica, Wetzlar, Germany).

3.8. Cell culture

THP-1 cells (TIB-202 [human monocytic cells]; ATCC, Manassas, VA, USA) were cultured in Roswell Park Memorial Institute 1640 medium (Corning Inc., New York, NY, USA) with 10% (v/v) fetal bovine serum (Gibco, Gaithersburg, MD, USA) and a 1% (w/v) antibiotic/antimycotic cocktail (HyClone, Logan, UT, USA) at 37 ºC under 5% CO_2. Culture media were replaced every 4-5 days. For NIH3T3 cells (CRL-1658 [mouse fibroblasts]; ATCC, Manassas, VA, USA) culture, Dulbecco's Modified Eagle's Medium (high glucose; Hyclone) with 10% (v/v) fetal bovine serum was used and replaced every 2-3 days. The other condition was same as THP-1 cell culture. For immature DCs, THP-1 cells were cultured for 6 days in RPMI medium supplemented with 100 ng/mL of GM-CSF and IL-4 (Woongbee Meditech Inc, Seoul, Korea).

Cytotoxicity of nanogels was evaluated as described previously [50]. THP-1 and NIH3T3 cells were seeded at concentrations of 2.5×10^4 cells/well in a 96-well plate and incubated for 48 h. Then the cells were treated with nanogels at 0-4×10^8 nanoparticles/mL for 24 h. After incubation, the cells were collected and washed with PBS, followed by trypan blue staining. Live and dead cell numbers were counted using a hemocytometer.

Relative metabolic activity was measured using a resazurin assay. THP-1 and NIH3T3 cells were cultured at 5×10^3 cells/well in a 96-well plate. After 48 h, 2.5 mg/mL resazurin solution diluted 100-fold in medium was

added to each well and the plate was incubated for 4 h. Fluorescence was measured using a microplate reader (excitation: 560 nm; emission: 590 nm; Synergy HT; BioTek, Winooski, VT, USA).

3.9. Fluorescence microscopy

The fluorescence of cryo-sectioned slices was observed under a fluorescence microscope (Cellena S; Logos Biosystems, Anyang, Korea). Image J software (ver.1.8.0_172; National Institutes of Health, Bethesda, MD, USA) was used to semi-quantitatively analyze fluorescence intensities using the relative fluorescence intensity approach. To visualize nanogel cellular uptake, THP-1 cells were incubated with rhodamine B-labeled OVA (100 ng/mL) and nanogels (4×10^8 nanoparticles/mL) for 24 h, rinsed three times with PBS, and observed under the fluorescence microscope.

3.10. Reverse transcription-quantitative polymerase chain reaction

Nanogel-treated cells were collected after 24 h and RNA extracted using a RNA kit (NucleoSpin; Macherey Nagel, Düren, Germany) following the manufacturer's protocol. Via reverse transcription (RT), RNA was converted into single-stranded cDNA using a kit (PrimeScript; TaKaRa, Kusatsu, Japan). Quantitative real-time polymerase chain reaction (RT-qPCR) was performed using a commercial qPCR premix (SYBR Premix Ex TaqII kit; TaKaRa) and a real-time platform (StepOne; Applied Biosystems, Foster City, CA, USA). PCR proceeded at 95 ºC for 30 s followed by 40 cycles of

Table 1. Primer sequences for qPCR

Gene	Primer sequence (5' to 3')	Reference
GAPDH	F-AGC CTC AAG ATC ATC AGC AAT G R-CAC GAT ACC AAA GTT GTC ATG GAT	[51]
HLA-DRA	F-TCG AAA TGG AAA ACC TGT CAC C R-CCC AAT AAT GAT GCC CAC CA	[52]
CD80	F-TGG TGC TGG CTG GTC TTT C R-CGT TGC CAC TTC TTT CAC TTC C	[53]
CD83	F-AGG TTC CCT ACA CGG TCT CC R-TTG CAG CTG GTA GTG TTT CG	[54]
CD86	F-GGG CCG CAC AAG TTT TGA R-GCC CTT GTC CTT GAT CTG AA	[55]

95 ºC for 5 s, 55 ºC for 30 s, and 72 ºC for 30 s. Amplified gene levels were normalized to those of GAPDH (internal control) and evaluated using the $2^{-\Delta\Delta CT}$ method. **Table 1** lists the forward and reverse primers.

3.11. Flow cytometry

Cultured nanogel-treated cells were collected and subjected to flow cytometry (BD Accuri; Becton Dickinson, Franklin Lakes, NJ, USA) to measure the fluorescence intensities of rhodamine B-labeled OVA and nanogels, and evaluate DC uptake. To assess DC maturation, cells were cultured and incubated with rhodamine B-labeled OVA, vehicle, and nanogel, as described previously. The cells were rinsed with PBS and fixed in 4% (w/v) paraformaldehyde (≥ 95%) for 10 min, followed by three washes. Fixed cells were permeabilized for 5 min in a 0.1% (w/v) saponin solution (original concentration = 8–25% w/v) and blocked in Tris-buffered saline with 1% (w/v) bovine serum albumin (BSA; ≥ 98%) for 30 min at room temperature. The cells were then stained with the recommended dilutions of fluorescent dye-conjugated monoclonal antibodies (Alexa Fluor 488 anti-human HLA-DR antibody and APC anti-human CD83 antibody; Biolegend; San Diego, CA, USA) in blocking buffer for 30 min at room temperature and washed with PBS containing 0.05% (v/v) Tween 20 (≥ 40%; Bio-Rad). Fluorescence shifts attributable to antibody-binding were evaluated by flow cytometry.

3.12. Statistics

All experiments were performed in triplicate, and data are presented as mean ± standard deviation unless otherwise stated. For multiple group comparisons, one-way ANOVA with the Bonferroni post-hoc test was performed. For between-group comparisons, Student's t-test was performed based on the results of the Shapiro-Wilk normality test and the F-test. P-values < 0.05, < 0.01, and < 0.001 were considered significant.

IV. RESULTS AND DISCUSSION

4.1. Formation and Characterization of OVA-tethered bulk pectin gels

To control the number of NB groups on the pectin chain, 5-norbornene-2-methylamine feed ratio was varied during synthesis (**Table 2**). **Figure 1** shows the pectin-NB structure and ^{1}H-NMR spectra of intact pectin and pectin-NB. Multiple NB peaks were evident at 1.3–6.2 ppm in pectin-NB samples [56], regardless of the feed ratio. To determine the numbers of NB molecules introduced, the peak areas from 6.0–6.2 and 5.0–5.1 ppm were compared [57,58]. The NB levels were 0.63, 0.72, and 0.96 mmol/g pectin at feed ratios of 1, 2, and 4 respectively. Fourier-transform infrared spectroscopy also revealed NB groups (**Figure 2A**). The intensity of bands attributable to carbonyl group stretching (1,610 and 1,408 cm-1) gradually increased with the feed ratio, while the band at 1,740 cm-1 (attributable to carbonyl group stretching of carboxylic acid) clearly decreased [56,59]. Thus, NB groups were successfully introduced into the pectin chain via EDC chemistry. Next, bulk gels of 1% (w/v) pectin-NB synthesized at different NB-methylamine feed ratios were formed and shear moduli were measured. The shear storage modulus increased significantly from a 1× to 2× feed ratio, whereas the shear storage moduli of the 2× and 4× feed ratio samples were similar (**Figure 2B**). Therefore, pectin-NB prepared at a 2× feed ratio was

used.

Table 2. Formulation for norbornene-modified pectin synthesis and the degree of norbornene modification of resulting pectin-NB

Feed ratio [a] (×)	EDC (mmol/g)[b]	5-Norbornene-2-methylamine (mmol/g)[b]	Degree of norbornene modification (mmol/g)[c]
1	2.81	5.63	0.63
2	5.63	11.25	0.72
4	11.25	22.50	0.96

[a] Equal molar amount of 5-norbornene-2-methylamine to galacturonic acid of pectin.
[b] Molar amount to 1 g of intact pectin.
[c] Molar amount to 1 g of pectin-NB, which was determined by ^{1}H-NMR spectrum.

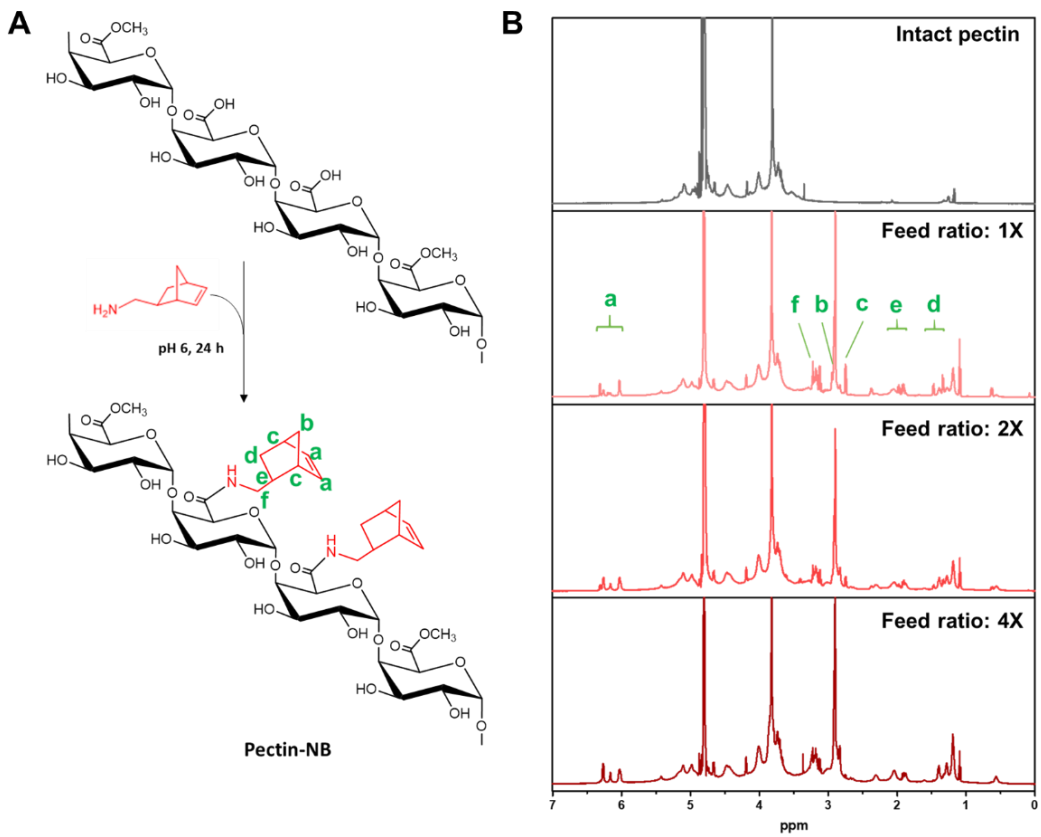

Figure 1. Synthesis and characterization of pectin-norbornene (pectin-NB). (A) Pectin-NB was synthesized by reaction with 5-Norbornene-2-methylamine. (B) ^{1}H-NMR spectra of intact pectin and its derivatives (pectin-NB). Pectin-NB 1X, 2X, and 4X was synthesized by adding 1, 2, and 4 equivalent of 5-Norbornene-2-methylamine respectively to the galacturonic acid of pectin. (a) 2H at δ = 6.02-6.2 ppm; (b) 2H at 2.9 ppm; (c) 1H at 2.7 ppm; (d) 2H at 1.3-1.5 ppm; (e) 1H at 1.9-2.1 ppm; (f) 2H at 3.4 ppm.

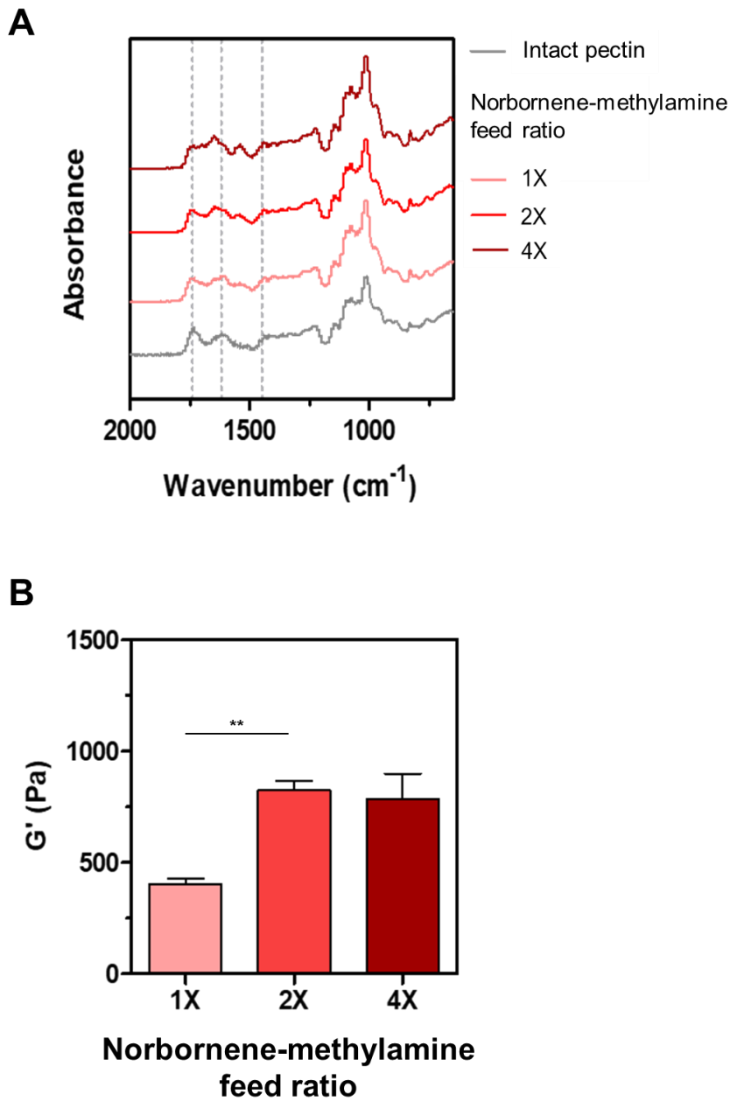

Figure 2. Characterization of pectin-NB according to concentration of pectin-NB. (A) FT-IR spectra of intact pectin and pectin-norbornene derivatives synthesized at different norbornene-methylamine feed ratios. (B) Shear storage moduli of pectin hydrogels formed with pectin-NB synthesized at different norbornene-methylamine feed ratios. The prepolymer solutions were prepared at 1% and a balanced stoichiometric ratio of DTT in the presence of 1 mM LAP (n = 3, mean ± standard deviation).

The bulk hydrogels (without OVA-SH) were fabricated at various DTT concentrations and the shear storage moduli were measured. The highest modulus was obtained when the NB and thiol groups were in stoichiometric balance (**Figure 3**), as predicted by the ^{1}H-NMR analysis. As shown in **Figure 4**, gelation occurred rapidly after UV light exposure at all concentrations; the shear modulus plateaued within 120 s, indicating that gelation was complete, regardless of the pectin-NB concentration. Prior to nanogel fabrication, OVA-SH loading efficiency in bulk gels was assessed (**Table 3**). **Figure 5A** shows the release profiles of OVA-SH from 0.1 mM-OVA-SH-incorporated pectin hydrogels in PBS. As expected, immobilized OVA-SH was released rapidly within 8 h, but the cumulative release plateaued at about 50% over the next 16 h, regardless of the pectin-NB concentration. It is speculated that OVA-SH release was attributable to an incomplete thiol-NB reaction, thus reflecting the complexity of OVA structure. **Figure 5B** shows the OVA loading efficiencies of bulk pectin gels exposed to various levels of OVA-SH (i.e., 0.1, 0.2, and 0.4 mM in the prepolymer solution). Notably, the loading efficiency increased by up to ~70% as the OVA-SH level in pectin gels increased from 1.0 to 2.0%, but was not high in the 0.5% pectin (w/v) gel. As the bulk hydrogel was decomposed, antigens could be released (**Figure 5C**). The fluorescence of OVA-SH-Rho was steadily released until 168 h in the presence 10 mg/mL of lysozyme than the condition without treatment. Due to the large surface area of nanogel, they will degrade faster than bulk hydrogels releasing OVA rapidly.

Table 3. Formulation of pectin-NB/OVA-SH hydrogels

Pectin-NB conc.	$[ene]_{NB}$ (mM)	$[SH]_{DTT}$ conc. (mM)	Residual $[ene]_{NB}$ (mM)	[OVA-SH] (mM)		
				0.1	0.2	0.4
				$[SH]_{OVA-SH}$ (mM)		
0.5%	3.5	2.5	1	0.36	0.71	1.42
1.0%	7	6	1	0.36	0.71	1.42
2.0%	14	13	1	0.36	0.71	1.42

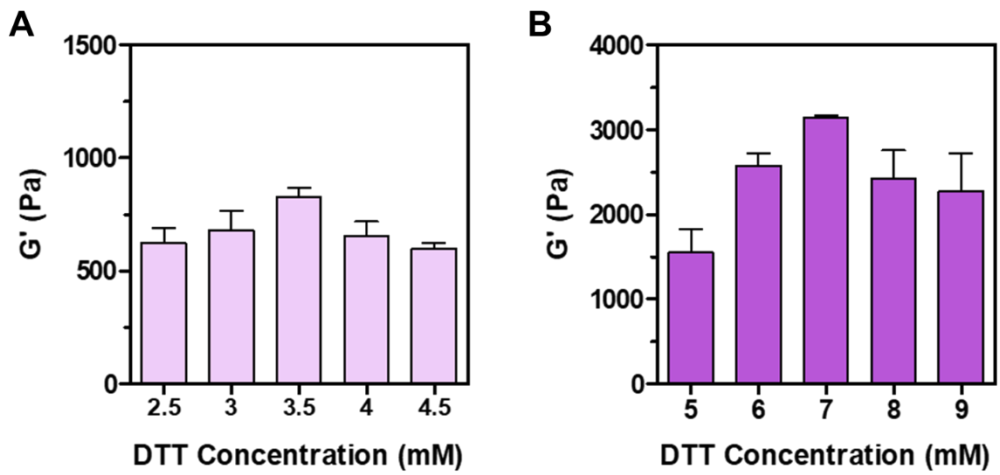

Figure 3. Shear storage modulus of (A) 1.0% and (B) 2.0% pectin hydrogels formed with different concentrations of DTT in prepolymer solutions. The shear modulus was measured at equilibrium swelling state after 24 h incubation in PBS (n = 3, mean ± standard deviation).

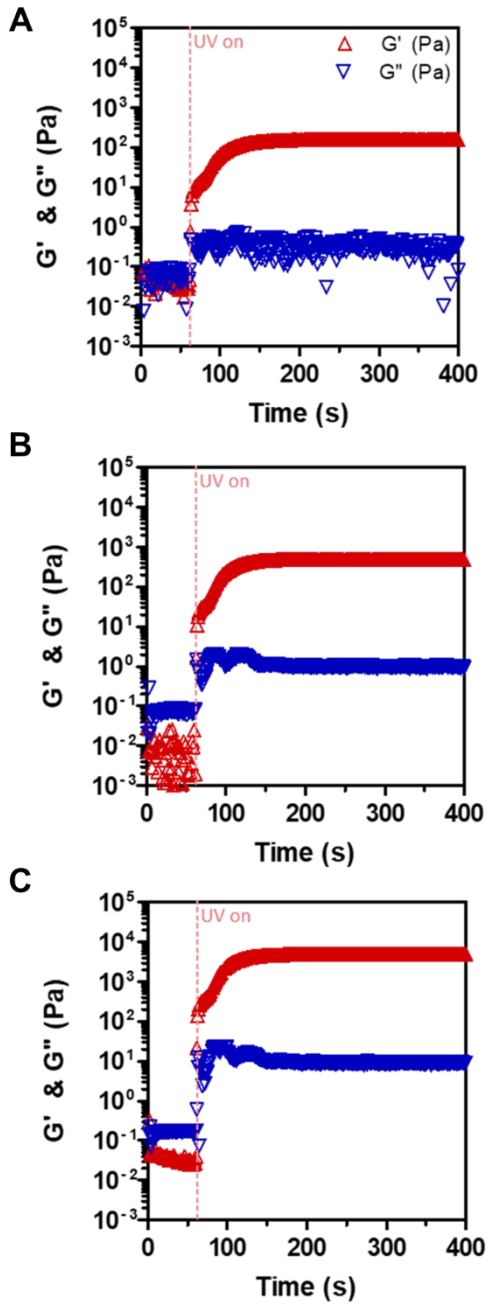

Figure 4. In situ photo-rheometry results of (A) 0.5%, (B) 1.0%, and (C) 2.0% pectin bulk hydrogels at strain sweep mode. The UV light was turned on at 60 s after the onset of measurement.

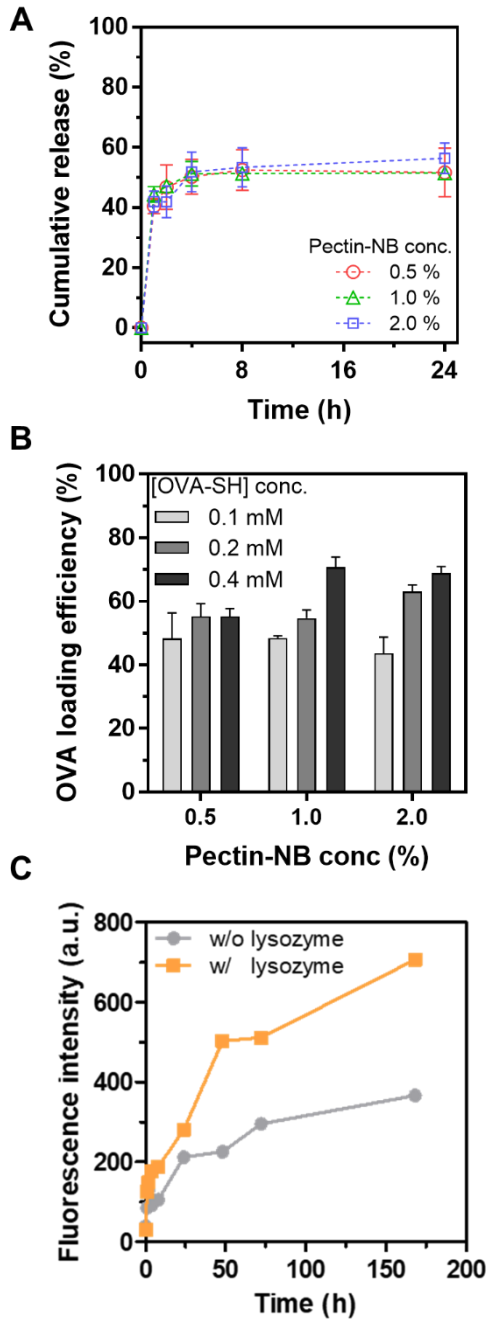

Figure 5. OVA-SH loading efficiency of pectin bulk hydrogels. (A) Cumulative amount of unfixed OVA-SH from pectin bulk hydrogels at 0.1 mM OVA-SH. (B) OVA loading efficiency of pectin bulk hydrogels at different OVA-SH concentrations after 24 h incubation. (C) Cumulative release of OVA-SH-Rho by degradation of pectin bulk hydrogels by lysozyme at 10 mg/mL concentration.

Taken together, precise control of protein loading could be achieved by modulating the amounts of hydrogel components.

Figure 6 shows the swelling ratios and gel fractions of pectin hydrogels formed in the presence or absence of OVA-SH (0.1 mM). The swelling ratio increased as the pectin-NB concentration increased, whereas the gel fraction decreased. OVA-SH incorporation affected only the gel fractions; the swelling ratios did not change. The reduced gel fraction on OVA-SH loaded nanogels was attributable to the release of untethered OVA-SH during crosslinking. The effects of OVA-SH on both the swelling ratio and shear modulus (**Figure 7A**) were negligible; OVA-SH did not compromise the reaction between pectin-NB and DTT (the cross linker). Thus, the crosslinking density was controlled only by the pectin-NB concentration and stoichiometric balance between the NB and DTT thiol groups (**Figure 7B**).

4.2. OVA-loaded pectin nanogel fabricated by ultrasonication

To prepare 1% (w/v) nanogels, the concentration of OVA-SH in the prepolymer solution was held constant (**Figure 5**) and nanogels were subjected to ultrasonication, as described previously [12]. **Figure 8** show the volume percentages in the range 100–300 nm, which allows skin penetration

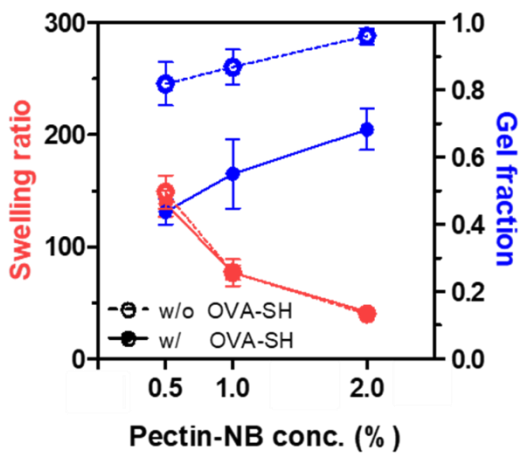

Figure 6. Swelling ratio and gel fraction of pectin hydrogels with or without OVA-SH.

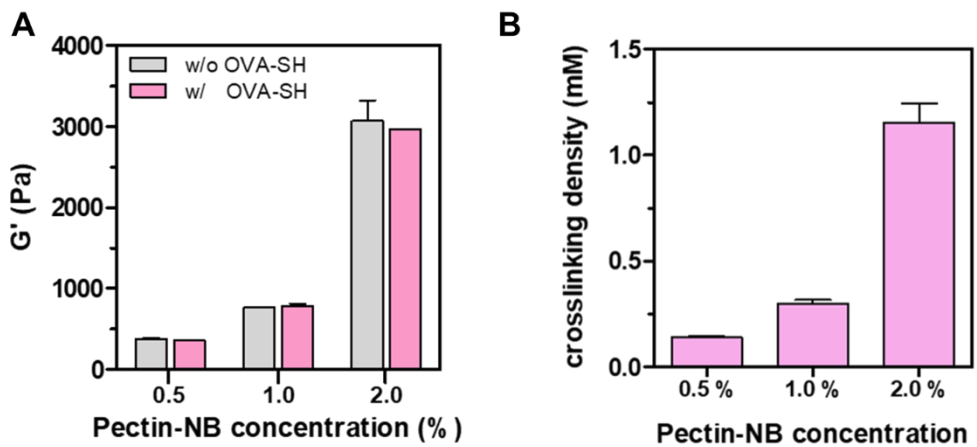

Figure 7. Physical properties of pectin bulk hydrogels. (A) Shear storage moduli of pectin hydrogels with or without OVA-SH. (B) Crosslinking densities of pectin hydrogels formed at various pectin concentrations (n = 3, mean ± standard deviation).

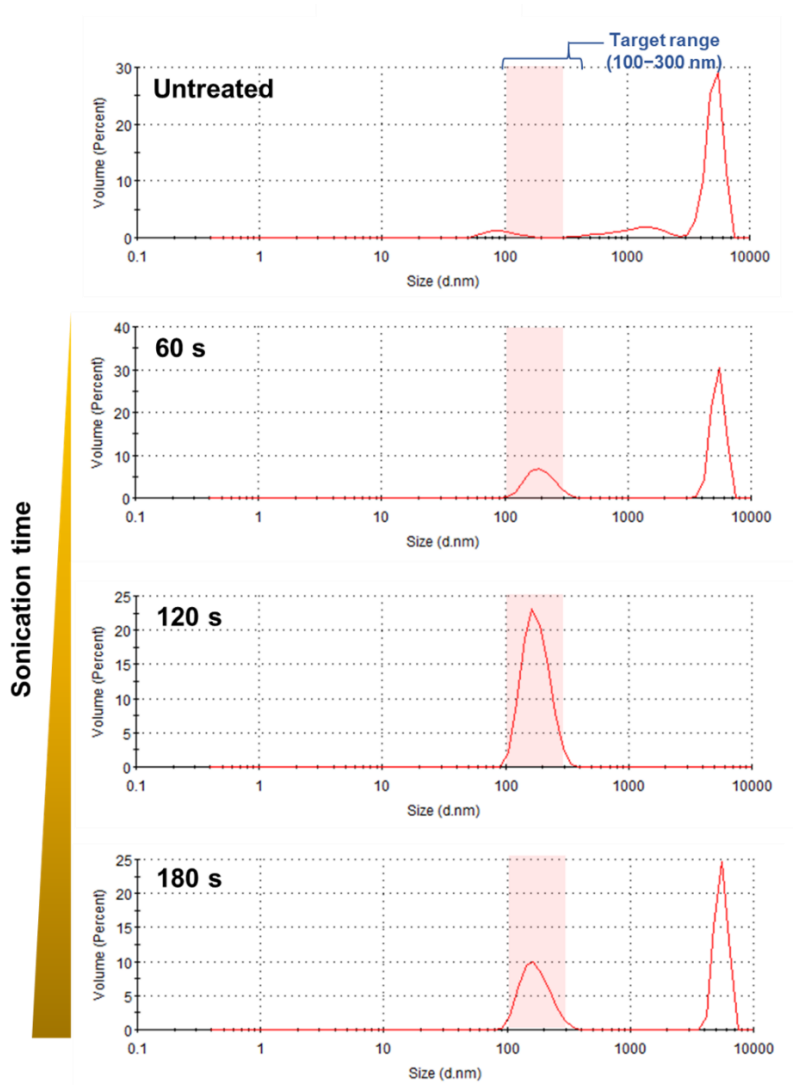

Figure 8. Distribution graph present in the 100-300 nm size range of 1.0% pectin nanogels according to ultra-sonication time.

[2,9,11]. The highest yield (~ 90%) was achieved at 120 s. It is consistent with the result of calculating the yield of the nanogel within the target range (**Figure 9A**). Next, the ultrasonic power was varied over 120 s. However, this had little effect on the volume fraction (**Figure 9B**). Thus, the ultrasonication process was fixed at 26 W for 120 s to minimize chain decomposition.

Filtration was performed through 0.45-μm-pore size syringe filters to remove debris, and the average nanogel sizes were compared. **Figure 10** shows that the as-formed pectin gels were micro-sized (~4 μm); the Z-average size decreased to ~200 nm after sonication and syringe filtration. In particular, even with only the sonication process, the z-average value was not significantly different from that of the filtration. This means that the optimization process is suitable for fabricating nanogels within the target range.

Next, pectin nanogels were prepared by varying the pectin-NB concentration under the conditions described above. To observe swollen nanogels, cryo-TEM was performed. **Figure 11** shows that the nanogels were ~200-nm-diameter spheres regardless of the pectin-NB concentration. However, the concentration of prepolymer solution affected the size distribution. In NTA results, the peak moved from 160 to 220 nm as the concentration increased (**Figure 12**). The distribution curve was very narrow at 1.0% (w/v) pectin, but broader at 0.5 and 2.0% (w/v) pectin, possibly because hydrogel stiffness affected the uniformity of nanogel size. Since

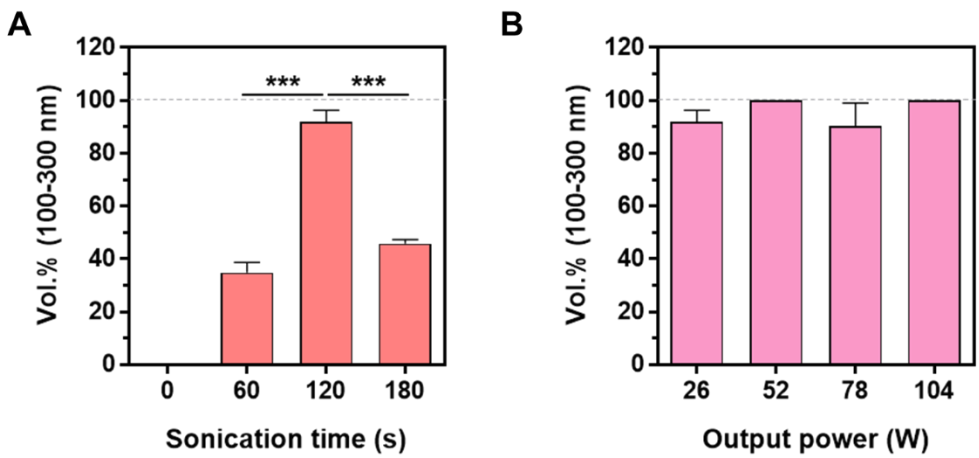

Figure 9. Volume ratio (%) present in the 100-300 nm size range of 1.0% pectin nanogels according to (A) ultra-sonication time and (B) ultra-sonication power.

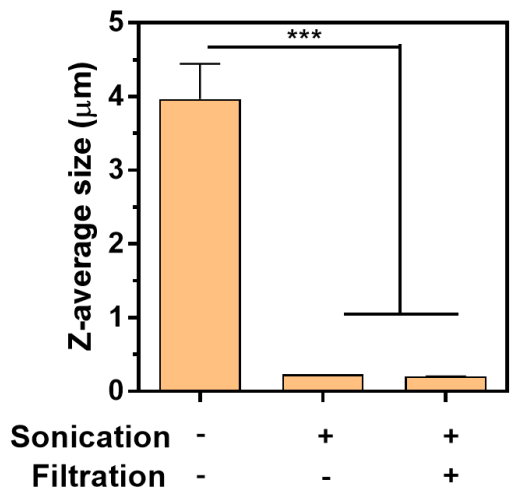

Figure 10. Z-average of 1.0% pectin nanogels fabricated by sonication and filtration. The particle size and Z-average were measured using a zetasizer.

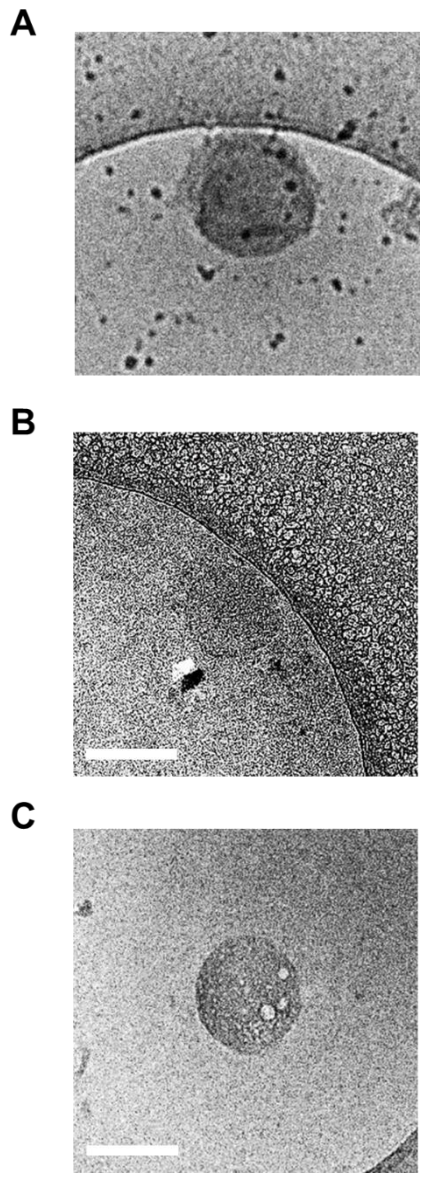

Figure 11. Cryo transmission electron microscopy images of (A) 0.5%, (B) 1.0%, and (C) 2.0% pectin nanogels. (Scale bar: 200 nm)

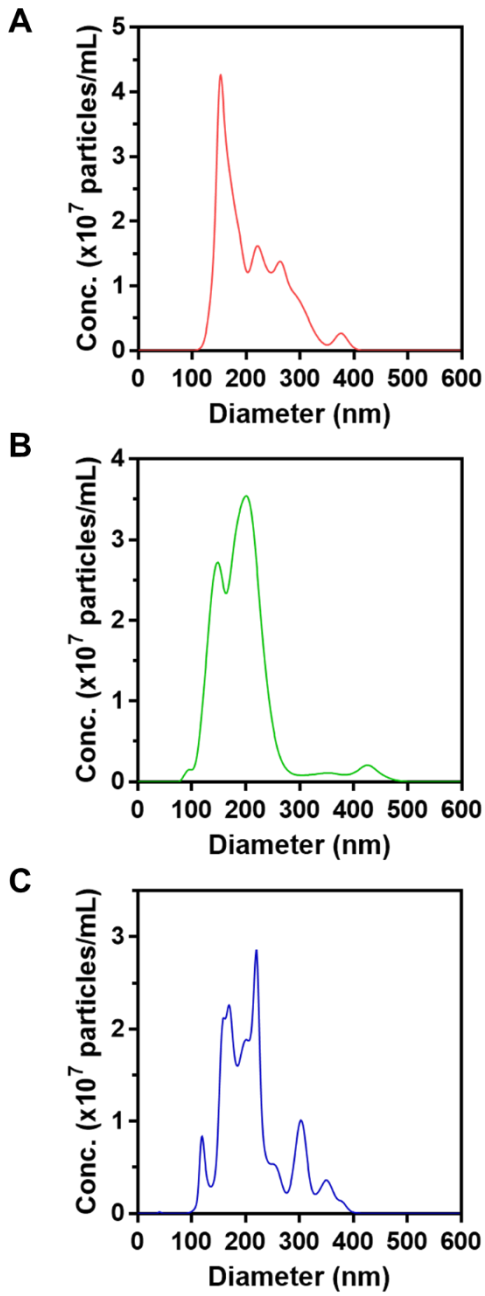

Figure 12. Distribution graph of (A) 0.5%, (B) 1.0%, and (C) 2.0% pectin nanogels. The particle size distributions were measured using a nanoparticle tracking analyzer.

sonication was performed under the same conditions regardless of the concentration of pectin-NB, the size of the 2.0% nanogel with relatively high physical properties is large, and the 0.5% nanogel with low physical properties is small.

Figure 13 shows the changes in the Z-average size of pectin nanogels under diverse conditions, including storage (4 and 25 ºC), application (32 ºC), and digestion (in lysozyme at 32 ºC). The Z-average sizes did not change significantly at 4 ºC over 8 days, but increased markedly at 25 ºC and 32 ºC. The negative charges of pectin nanogels were gradually eliminated as the temperature increased (**Figure 14**). It might be due to changes in the dissociation constant of pectin carboxylic groups and it led to aggregation of nanogels [60]. Therefore, storage at 4 ºC is optimal; the nanogel size remains appropriate for skin application.

For effective antigen delivery, the carrier should be rapidly digested by phagocytes on delivery to a target tissue. **Figure 15** shows dramatic Z-average size changes of nanogels within 48 h of incubation with lysozyme (10 mg/mL). The sizes of 0.5 and 1.0% (w/v) pectin nanogels increased rapidly over the first 8 h and then gradually decreased. It is speculated that this reflected dual-mode degradation (bulk degradation and surface erosion). Initially, lysozyme reduced crosslinking by hydrolyzing the pectin chain, triggering swelling. After 8 h, surface erosion predominated and the nanogels concentration. At higher concentrations, the changes were relatively small,

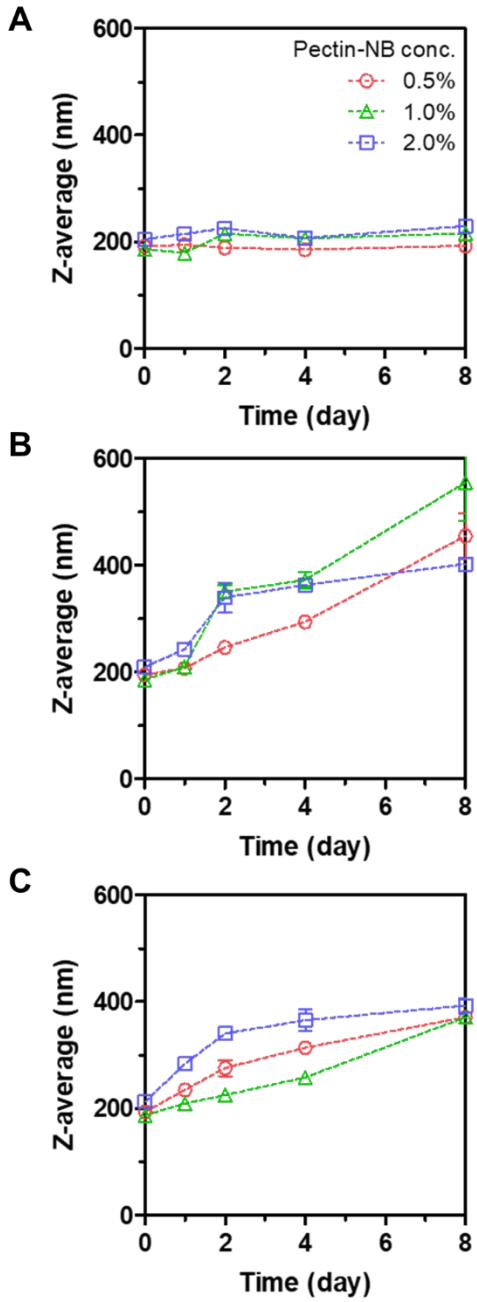

Figure 13. Stability of pectin nanogels. Z-average size changes of nanogels incubated in phosphate-buffered saline at (A) 4 ºC, (B) 25 ºC, and (C) 32 ºC.

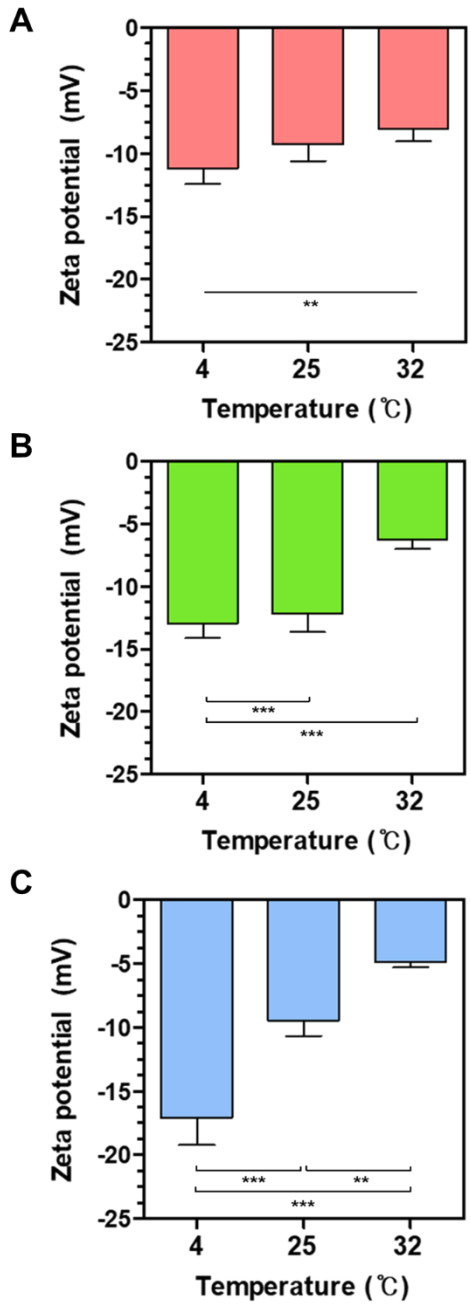

Figure 14. Zeta potentials of pectin nanogels in PBS at different temperatures. (A) 0.5%, (B) 1.0%, and (C) 2.0% pectin nanogels (n = 3, mean ± standard deviation).

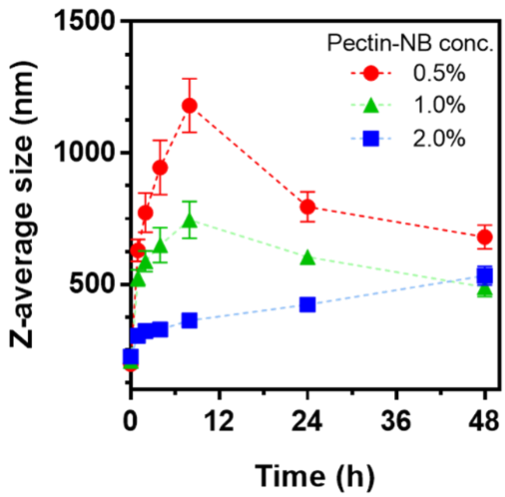

Figure 15. Degradation of pectin nanogels. Z-average size changes of pectin nanogels incubated in phosphate-buffered under the condition of lysozyme treatment at 10 mg/mL concentration.

decreased in size [61,62]. The size changes were affected by the pectin-NB indicating that the antigen release rate can be controlled by modulating the crosslinking density. The pectin nanogel is expected to be degraded by the lysozyme of the lysosome after internalization into the cell and release internal antigen.

4.3. Porcine skin penetration by pectin nanogels

Figure 16 shows fluorescence images of porcine skin cross-sections 24 h after treatment with rhodamine B-labeled pectin nanogels. Prior to the test, the skin penetration of soluble OVA-Rho and pectin-Rho were examined. As expected, OVA-Rho barely reached the dermis; most remained in the SC at 24 h post-treatment, consistent with the results of previous studies [12,13]. Pectin-Rho yielded faint dermal fluorescence, and strong fluorescence of the SC and epidermis; pectin penetrated the SC layer. As stated above, this may be because pectin is physicochemically similar to HA. Pectin can be extensively hydrated, but is amphiphilic in nature albeit that the structure is less regular than that of HA [15,42]. Thus, it is assumed that pectin penetrates the skin via a mechanism similar to that of HA.

In the pectin nanogel-treated groups, fluorescence was evident over the entire cross-section (SC, epidermis, and dermis) of skin, regardless of the pectin-NB concentration. The dermal fluorescence intensity was higher than that of the pectin-Rho group; the nanogel penetrated the skin better than

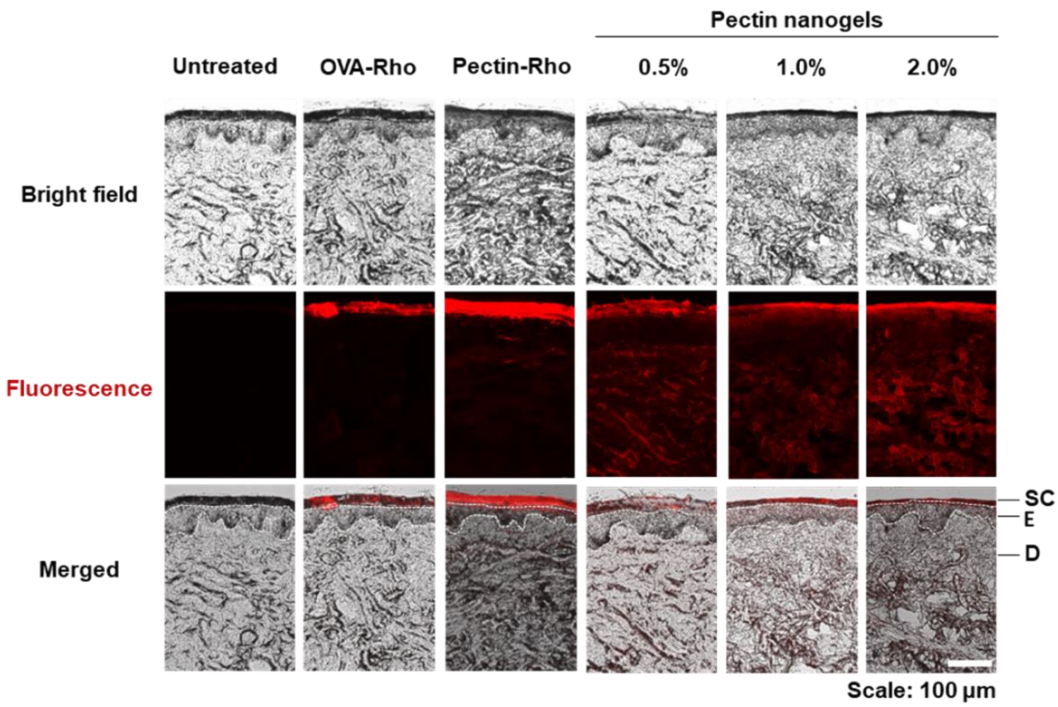

Figure 16. Porcine skin penetration test of rhodamine B-labeled OVA, pectin solutions, and pectin nanogels. Bright-field and fluorescence images of histological sections of porcine skin after 24 h incubation.

soluble pectin, attributable to both its elasticity and large surface area. The nanogel became extensively hydrated in the SC layer and then infiltrated the cells.

For a more detailed comparison of skin penetrability, the relative fluorescence intensities were measured (**Figure 17**). The dermal fluorescence intensities of soluble pectin and pectin nanogels were high, whereas ~90% of OVA-Rho fluorescence was seen in the SC. Interestingly, in the nanogel-treated groups, the relative dermal fluorescence intensity increased as the pectin-NB concentration increased, indicating that relatively larger amounts (compared to OVA-SH-Rho) of nanogels reached the dermis, regardless of the pectin-NB concentration. It is assumed that both the elasticity and the presence of hydrophobic NB groups play important roles in skin penetration. According to the research results, the elasticity of nanoparticles such as transferosome can affect the skin permeability [33,63]. Besides, as shown in **Figure 6**, the water content of the hydrogel decreased at a high concentration of pectin. It might enhance the skin permeability [33-35,64].

In summary, transcutaneous delivery could be controlled by modulating the nanogel crosslinking density. The skin penetration mechanism of pectin nanogels should be further studied using different pectin. However, it is clear that pectin nanogels provide excellent transcutaneous delivery without the need for ethanol treatment or tape stripping.

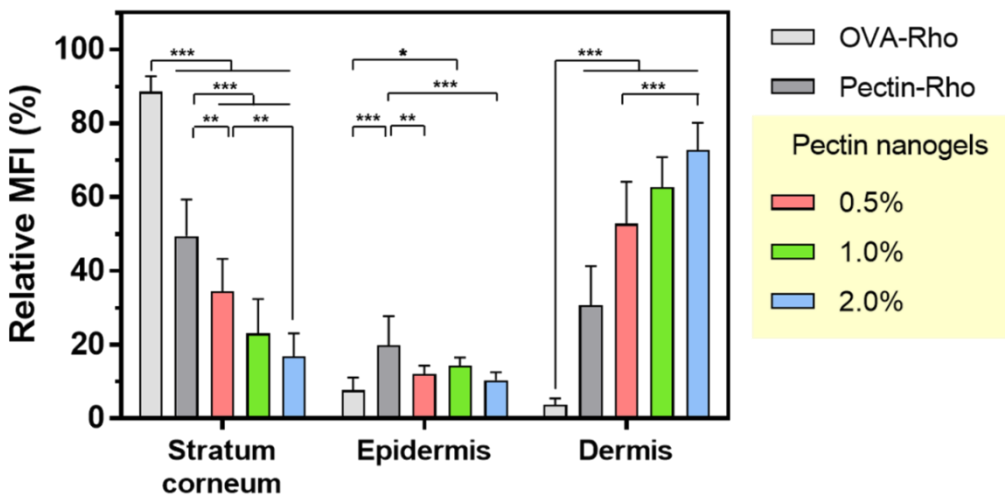

Figure 17. Semi-quantitative analysis of skin penetration amount of rhodamine B-labeled OVA, pectin solutions, and pectin nanogels.

4.4. DC uptake of pectin nanogels and cell maturation

Nanogels at 1% (w/v) (6.25–400 × 10^6 particles/mL) were not toxic to NIH3T3 fibroblasts or THP-1 monocytes (**Figure 18** and **Figure 19**). Thus, nanogels (vehicle and OVA-tethered) at 400 × 10^6 particles/mL were added to THP-1-derived immature DCs (iDCs) (**Figure 20**). All fluorescence was internalized by the iDCs; nanogels with and without OVA did not compromise uptake, possibly due to TLR-mediated phagocytosis [17,65,66]. Meanwhile, minute morphology changes of iDCs were observed in the pectin nanogels-treated groups [67,68]. It is presumed that the maturation of iDCs occurred due to nanogel internalization.

The levels of mRNAs encoding DC maturation markers were measured 24 h after nanogel uptake. The levels of mRNAs encoding HLA-DRA, CD80, and CD83 increased in iDCs treated with OVA-loaded nanogels, but the level of mRNA encoding CD86 did not (**Figure 21**). Thus, the DC phenotype was not affected by nanogel treatment [26,69,70]. Interestingly, the CD80 and CD83 expression levels increased slightly even in the vehicle group, indicating that pectin co-stimulated DC maturation [71-73]. The elevated expression of HLA-DRA and CD83 indicate activation of the antigen key for MHC-II/peptide complex formation and T-cell activation [74,75]. The flow cytometry data were consistent with these observations. In addition, a significant increase in the HLA-DRA/CD83-positive cell

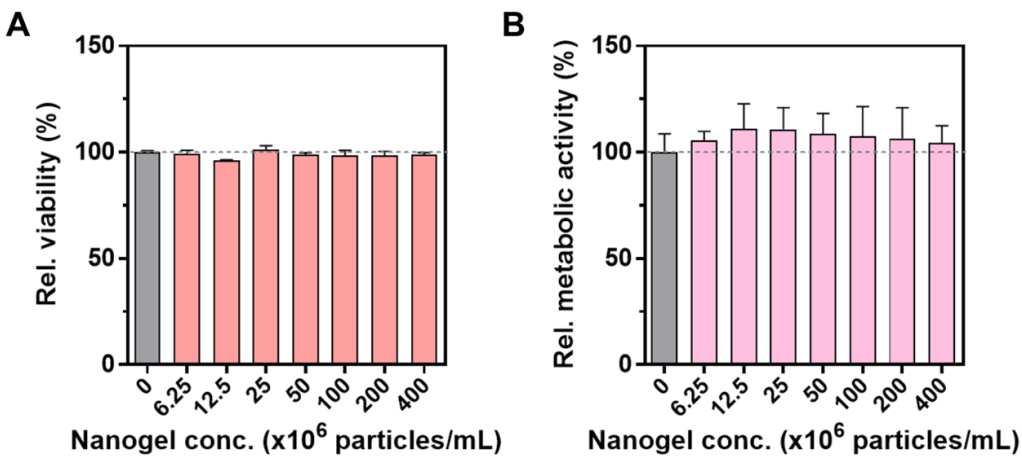

Figure 18. Result of cytotoxicity test of pectin nanogels formed with 1% pectin prepolymer solution on NIH3T3 cells. (A) Relative viability; (B) relative metabolic activity (n = 3, mean ± standard deviation).

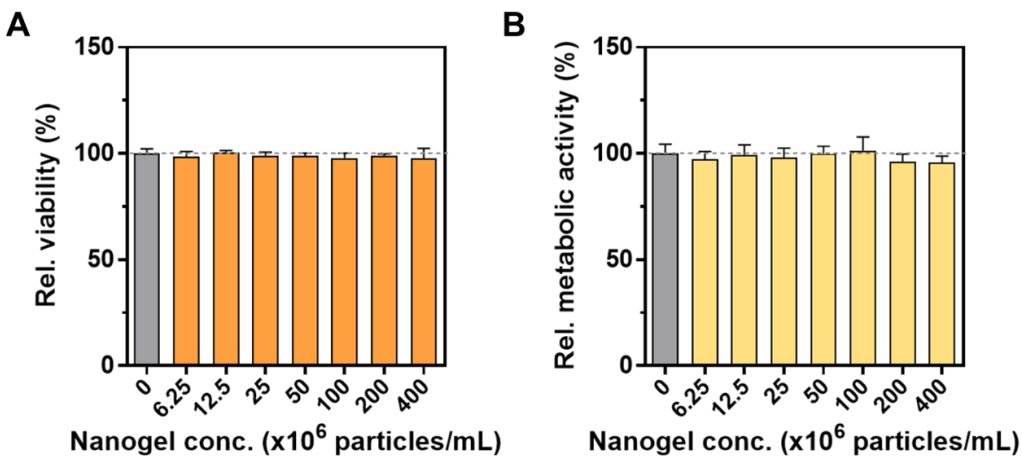

Figure 19. Result of cytotoxicity test of pectin nanogels formed with 1% pectin prepolymer solution on THP-1 cells. (A) Relative viability; (B) relative metabolic activity (n = 3, mean ± standard deviation).

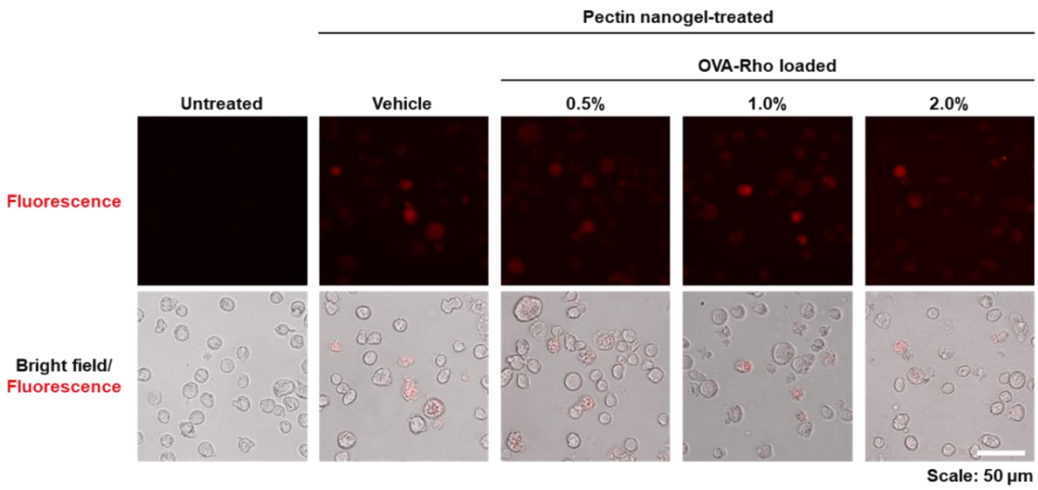

Figure 20. Fluorescence microscope images of rhodamine B-labeled pectin vehicle and pectin nanogels internalized by THP-1 iDC.

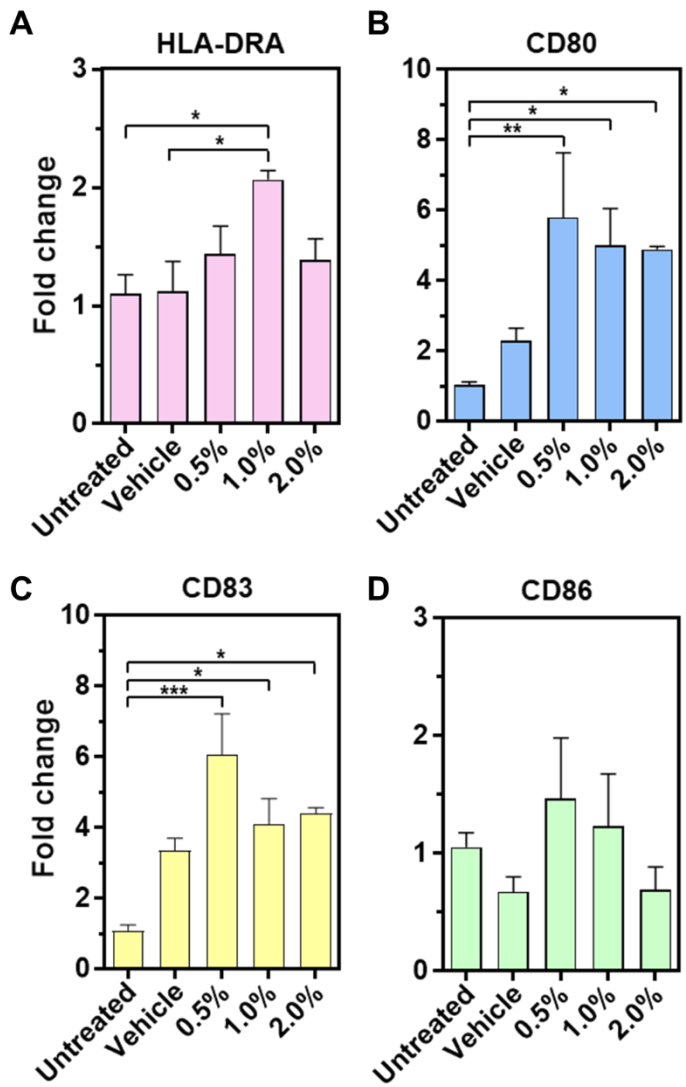

Figure 21. Relative mRNA expression levels of (A) HLA-DRA, (B) CD80, (C) CD83, and (D) CD86 in cells treated with 1.0% pectin vehicles and pectin nanogels. (n=9, mean ± standard error of mean).

population was evident in the OVA-loaded pectin nanogels treated group (**Figure 22**). It suggests that loaded OVA and pectin nanogel itself synergistically activated iDCs, resulted in better antigen presentation [26,69-75].

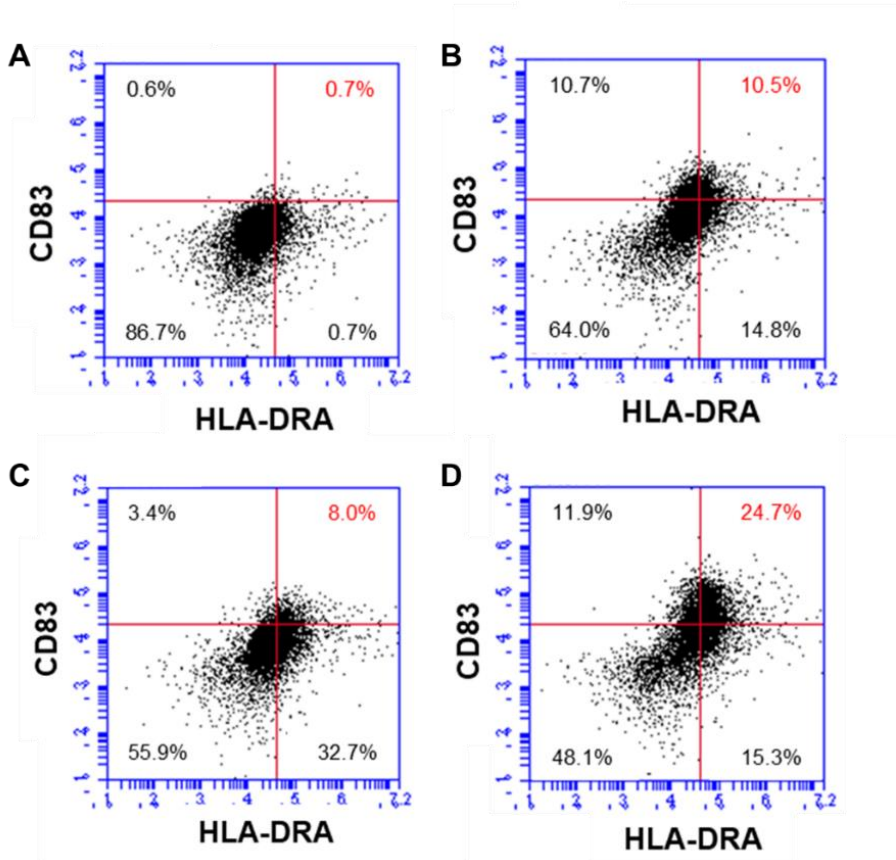

Figure 22. Flow cytometry results of THP-1 iDC with (A) untreated, and treated with (B) OVA, (C) 1.0% pectin nanogels (vehicles), and (D) OVA-loaded 1.0% pectin nanogels. All the cells were stained with both HLA-DRA and CD83.

V. CONCLUSION

In summary, OVA-loaded nanogels composed of norbornene functionalized pectin were fabricated via thiol-ene photo-click reaction and ultrasonication. The nanogels had an average diameter of 200 nm and a narrow size distribution. OVA was loaded to hydrogels by tethering OVA to the pectin network at various stoichiometric ratios. Fabricated pectin nanogels could display various OVA release behaviors by regulating crosslinking density. Porcine skin penetration test showed that soluble pectin and, in particular, the pectin nanogel reached the dermis of skin. Especially nanogels showed better skin penetration than soluble pectin, which is supposed to be elasticity or water content of nanogels. Pectin crosslinking density affected not only enzymatic degradation, but also transcutaneous delivery efficiency. OVA-loaded pectin nanogels were internalized by iDCs and synergistically upregulated the synthesis of maturation markers (i.e., HLA-DRA and CD83). This is the first study to describe skin penetration of pectin from citrus peel and modified pectin nanogels, suggesting that antigen-loaded pectin nanogels can be used for transcutaneous immunization.

VI. REFERENCES

[1] Bolzinger, M. A., Briançon, S., Pelletier, J., & Chevalier, Y. (2012). Penetration of drugs through skin, a complex rate-controlling membrane. Current Opinion in Colloid & Interface Science, 17(3), 156-165.

[2] Zhao, Z., Ukidve, A., Dasgupta, A., & Mitragotri, S. (2018). Transdermal immunomodulation: Principles, advances and perspectives. Advanced Drug Delivery Reviews, 127, 3-19.

[3] Szczepanik, M., & Majewska-Szczepanik, M. (2016). Transdermal immunotherapy: past, present and future. Pharmacological Reports, 68(4), 773-781.

[4] Chauhan, R. S., & Singh, G. K. (2001). Immunomodulation: An overview. Journal of Immunology and Immunopathology, 3(2), 1-15.

[5] Lee, M. Y., Shin, M. C., & Yang, V. C. (2013). Transcutaneous antigen delivery system. BMB Reports, 46(1), 17.

[6] Gamazo, C., Pastor, Y., Larrañeta, E., Berzosa, M., Irache, J. M., & Donnelly, R. F. (2019). Understanding the basis of transcutaneous vaccine delivery. Therapeutic Delivery, 10(1), 63-80.

[7] Naik, A., Kalia, Y. N., & Guy, R. H. (2000). Transdermal drug delivery: overcoming the skin's barrier function. Pharmaceutical Science & Technology Today, 3(9), 318-326.

[8] Carter, P., Narasimhan, B., & Wang, Q. (2019). Biocompatible nanoparticles and vesicular systems in transdermal drug delivery for various skin diseases. International Journal of Pharmaceutics, 555, 49-62.

[9] Hua, S. (2015). Lipid-based nano-delivery systems for skin delivery of drugs and bioactives. Frontiers in Pharmacology, 6, 219.

[10] Ye, J., Wang, Q., Zhou, X., & Zhang, N. (2008). Injectable actarit-loaded solid lipid nanoparticles as passive targeting therapeutic agents for rheumatoid arthritis. International Journal of Pharmaceutics, 352(1-2), 273-279.

[11] Yadav, H. K. S., Al Halabi, N. A., & Alsalloum, G. A. (2017). Nanogels as novel drug delivery systems-a review. Journal of Pharmacology & Pharmaceutical Research, 1(5).

[12] Kim, H., Lee, S., & Ki, C. S. (2021). Modular formation of hyaluronic acid/β-glucan hybrid nanogels for topical dermal delivery targeting skin dendritic cells. Carbohydrate Polymers, 252, 117132.

[13] Kim, K. S., Kim, H., Park, Y., Kong, W. H., Lee, S. W., Kwok, S. J., Hahn, S. K., & Yun, S. H. (2016). Noninvasive transdermal vaccination using

hyaluronan nanocarriers and laser adjuvant. Advanced Functional Materials, 26(15), 2512-2522.

[14] Yang, J. A., Kim, E. S., Kwon, J. H., Kim, H., Shin, J. H., Yun, S. H., Choi, K. Y., & Hahn, S. K. (2012). Transdermal delivery of hyaluronic acid–human growth hormone conjugate. Biomaterials, 33(25), 5947-5954.

[15] Munarin, F. A. B. I. O. L. A., Tanzi, M. C., & Petrini, P. A. O. L. A. (2012). Advances in biomedical applications of pectin gels. International Journal of Biological Macromolecules, 51(4), 681-689.

[16] Liang, R. H., Wang, L. H., Chen, J., Liu, W., & Liu, C. M. (2015). Alkylated pectin: synthesis, characterization, viscosity and emulsifying properties. Food Hydrocolloids, 50, 65-73.

[17] Ishisono, K., Yabe, T., & Kitaguchi, K. (2017). Citrus pectin attenuates endotoxin shock via suppression of Toll-like receptor signaling in Peyer's patch myeloid cells. The Journal of Nutritional Biochemistry, 50, 38-45.

[18] Prado, S. B., Beukema, M., Jermendi, E., Schols, H. A., de Vos, P., & Fabi, J. P. (2020). Pectin interaction with immune receptors is modulated by ripening process in papayas. Scientific Reports, 10(1), 1-11.

[19] Shin, M. S., Park, S. B., & Shin, K. S. (2018). Molecular mechanisms of immunomodulatory activity by polysaccharide isolated from the peels of

Citrus unshiu. International Journal of Biological Macromolecules, 112, 576-583.

[20] Khalil, D. N., Smith, E. L., Brentjens, R. J., & Wolchok, J. D. (2016). The future of cancer treatment: immunomodulation, CARs and combination immunotherapy. Nature Reviews Clinical Oncology, 13(5), 273-290.

[21] Ita, K. (2016). Transdermal delivery of vaccines–Recent progress and critical issues. Biomedicine & Pharmacotherapy, 83, 1080-1088.

[22] Kong, W. H., Sung, D. K., Kim, H., Yang, J. A., Ieronimakis, N., Kim, K. S., Lee, J., Kim, D. H., Yun, S. H., & Hahn, S. K. (2016). Self-adjuvanted hyaluronate–antigenic peptide conjugate for transdermal treatment of muscular dystrophy. Biomaterials, 81, 93-103.

[23] Matsuo, K., Hirobe, S., Okada, N., & Nakagawa, S. (2013). Frontiers of transcutaneous vaccination systems: novel technologies and devices for vaccine delivery. Vaccine, 31(19), 2403-2415.

[24] Karande, P., & Mitragotri, S. (2010). Transcutaneous immunization: an overview of advantages, disease targets, vaccines, and delivery technologies. Annual Review of Chemical and Biomolecular Engineering, 1, 175-201.

[25] Toyoda, M., Hama, S., Ikeda, Y., Nagasaki, Y., & Kogure, K. (2015). Anti-cancer vaccination by transdermal delivery of antigen peptide-loaded

nanogels via iontophoresis. International Journal of Pharmaceutics, 483(1-2), 110-114.

[26] Gardner, A., & Ruffell, B. (2016). Dendritic cells and cancer immunity. Trends in Immunology, 37(12), 855-865.

[27] Sato, K., & Fujita, S. (2007). Dendritic cells-nature and classification. Allergology International, 56(3), 183-191.

[28] Kapsenberg, M. L. (2003). Dendritic-cell control of pathogen-driven T-cell polarization. Nature Reviews Immunology, 3(12), 984-993.

[29] Klechevsky, E., Morita, R., Liu, M., Cao, Y., Coquery, S., Thompson-Snipes, L., Briere, F., Chaussabel, D., Zurawski, G., Palucka, A. K., Reiter, Y., Banchereau, J., & Ueno, H. (2008). Functional specializations of human epidermal Langerhans cells and CD14+ dermal dendritic cells. Immunity, 29(3), 497-510.

[30] Kozaka, S., Tahara, Y., Wakabayashi, R., Nakata, T., Ueda, T., Kamiya, N., & Goto, M. (2019). Transcutaneous cancer vaccine using a reverse micellar antigen carrier. Molecular Pharmaceutics, 17(2), 645-655.

[31] Bartosova, L., & Bajgar, J. (2012). Transdermal drug delivery in vitro using diffusion cells. Current Medicinal Chemistry, 19(27), 4671-4677.

[32] Naik, A., Kalia, Y. N., & Guy, R. H. (2000). Transdermal drug delivery: overcoming the skin's barrier function. Pharmaceutical Science & Technology Today, 3(9), 318-326.

[33] Chacko, I. A., Ghate, V. M., Dsouza, L., & Lewis, S. A. (2020). Lipid vesicles: A versatile drug delivery platform for dermal and transdermal applications. Colloids and Surfaces B: Biointerfaces, 111262.

[34] Sakdiset, P., Okada, A., Todo, H., & Sugibayashi, K. (2018). Selection of phospholipids to design liposome preparations with high skin penetration-enhancing effects. Journal of Drug Delivery Science and Technology, 44, 58-64.

[35] Mishra, V., Bansal, K. K., Verma, A., Yadav, N., Thakur, S., Sudhakar, K., & Rosenholm, J. M. (2018). Solid lipid nanoparticles: Emerging colloidal nano drug delivery systems. Pharmaceutics, 10(4), 191.

[36] Son, S. U., Lim, J. W., Kang, T., Jung, J., & Lim, E. K. (2017). Hyaluronan-based nanohydrogels as effective carriers for transdermal delivery of lipophilic agents: Towards transdermal drug administration in neurological disorders. Nanomaterials, 7(12), 427.

[37] Toyoda, M., Hama, S., Ikeda, Y., Nagasaki, Y., & Kogure, K. (2015). Anti-cancer vaccination by transdermal delivery of antigen peptide-loaded nanogels via iontophoresis. International Journal of Pharmaceutics, 483(1-2), 110-114.

[38] Li, D., Sun, F., Bourajjaj, M., Chen, Y., Pieters, E. H., Chen, J., van den Dikkenberg, J. B., Lou, B., Camps, M. G. M., Ossendorp, F., Hennink, W. E., Vermonden, T., & Van Nostrum, C. F. (2016). Strong in vivo antitumor responses induced by an antigen immobilized in nanogels via reducible bonds. Nanoscale, 8(47), 19592-19604.

[39] Nochi, T., Yuki, Y., Takahashi, H., Sawada, S. I., Mejima, M., Kohda, T., Harada, N., Kong, I. G., Sato, A., Kataoka, N., Tokuhara, D., Kurokawa, S., Takahashi, Y., Tsukada, H., Kozaki, S., Akiyoshi, K., & Kiyono, H. (2010). Nanogel antigenic protein-delivery system for adjuvant-free intranasal vaccines. Nature Materials, 9(7), 572-578.

[40] Lee, S., Park, Y. H., & Ki, C. S. (2016). Fabrication of PEG–carboxymethylcellulose hydrogel by thiol-norbornene photo-click chemistry. International Journal of Biological Macromolecules, 83, 1-8.

[41] Jung, H. S., Kim, K. S., Yun, S. H., & Hahn, S. K. (2014). Enhancing the transdermal penetration of nanoconstructs: could hyaluronic acid be the key?. Nanomedicine, 9(6), 743-745.

[42] Fallacara, A., Baldini, E., Manfredini, S., & Vertuani, S. (2018). Hyaluronic acid in the third millennium. Polymers, 10(7), 701.

[43] Liang, R. H., Wang, L. H., Chen, J., Liu, W., & Liu, C. M. (2015). Alkylated pectin: synthesis, characterization, viscosity and emulsifying properties. Food Hydrocolloids, 50, 65-73.

[44] Morris, V. J., Belshaw, N. J., Waldron, K. W., & Maxwell, E. G. (2013). The bioactivity of modified pectin fragments. Bioactive Carbohydrates and Dietary Fibre, 1(1), 21-37.

[45] Beukema, M., Faas, M. M., & de Vos, P. (2020). The effects of different dietary fiber pectin structures on the gastrointestinal immune barrier: impact via gut microbiota and direct effects on immune cells. Experimental & Molecular Medicine, 52(9), 1364-1376.

[46] Olejnik, J., Hume, A. J., & Mühlberger, E. (2018). Toll-like receptor 4 in acute viral infection: Too much of a good thing. PLoS Pathogens, 14(12), e1007390.

[47] Cen, X., Liu, S., & Cheng, K. (2018). The role of toll-like receptor in inflammation and tumor immunity. Frontiers in Pharmacology, 9, 878.

[48] Salatin, S., & Yari Khosroushahi, A. (2017). Overviews on the cellular uptake mechanism of polysaccharide colloidal nanoparticles. Journal of Cellular and Molecular Medicine, 21(9), 1668-1686.

[49] Yu, M., Chen, Z., Guo, W., Wang, J., Feng, Y., Kong, X., & Hong, Z. (2015). Specifically targeted delivery of protein to phagocytic macrophages. International Journal of Nanomedicine, 10, 1743.

[50] Lee, S., Tae, H., & Ki, C. S. (2017). Fabrication of schizophyllan hydrogel via orthogonal thiol-ene photopolymerization. Carbohydrate Polymers, 167, 270-279.

[51] Zhang, J., Kong, X., Zhang, Y., Sun, W., Xu, E., & Chen, X. (2020). Mdm2 is a target and mediator of IRP2 in cell growth control. The FASEB Journal, 34(2), 2301-2311.0

[52] Xu, L., Niesen, M. I., & Blanck, G. (2009). Linkage of a tumor immune function and cell cycle de-regulation via a gene regulatory network subcircuit. Molecular Immunology, 46(4), 569-575.

[53] Son, Y., Choi, J., Kim, B., Park, Y. C., Eo, S. K., Cho, H. R., Bae, S. S., Kim, C. D., & Kim, K. (2019). Cyclosporin A inhibits differentiation and activation of monocytic cells induced by 27-hydroxycholesterol. International Immunopharmacology, 69, 358-367.

[54] Sanarico, N., Colone, A., Grassi, M., Speranza, V., Giovannini, D., Ciaramella, A., Colizzi, V., & Mariani, F. (2011). Different transcriptional profiles of human monocyte-derived dendritic cells infected with distinct strains of Mycobacterium tuberculosis and Mycobacterium bovis bacillus Calmette-Guerin. Clinical and Developmental Immunology, 2011.

[55] Gautam, S., Fatehchand, K., Elavazhagan, S., Reader, B. F., Ren, L., Mo, X., Byrd, J. C., Tridandapani, Su., & Butchar, J. P. (2016). Reprogramming

nurse-like cells with interferon γ to interrupt chronic lymphocytic leukemia cell survival. Journal of Biological Chemistry, 291(27), 14356-14362.

[56] Li, N., Wang, H., Qu, X., & Chen, Y. (2017). Synthesis of Poly (norbornene-methylamine), a Biomimetic of Chitosan, by Ring-Opening Metathesis Polymerization (ROMP). Marine Drugs, 15(7), 223.

[57] Pereira, R. F., Barrias, C. C., Bártolo, P. J., & Granja, P. L. (2018). Cell-instructive pectin hydrogels crosslinked via thiol-norbornene photo-click chemistry for skin tissue engineering. Acta Biomaterialia, 66, 282-293.

[58] Wang, Y., Rapakousiou, A., & Astruc, D. (2014). ROMP synthesis of cobalticenium–enamine polyelectrolytes. Macromolecules, 47(12), 3767-3774.

[59] Ishak, K. M. K., Ahmad, Z., & Akil, H. M. (2010). Synthesis and characterization of cis-5-norbornene-2, 3-dicarboxylic anhydride-chitosan. e-Polymers, 10(1).

[60] Light, T. S. (1984). Temperature dependence and measurement of resistivity of pure water. Analytical Chemistry, 56(7), 1138-1142.

[61] Van Thienen, T. G., Lucas, B., Flesch, F. M., Van Nostrum, C. F., Demeester, J., & De Smedt, S. C. (2005). On the synthesis and characterization of biodegradable dextran nanogels with tunable degradation properties. Macromolecules, 38(20), 8503-8511.

[62] Wooster, T. J., Acquistapace, S., Mettraux, C., Donato, L., & Dekkers, B. L. (2019). Hierarchically structured phase separated biopolymer hydrogels create tailorable delayed burst release during gastrointestinal digestion. Journal of Colloid and Interface Science, 553, 308-319.

[63] Benson, H. A. (2006). Transfersomes for transdermal drug delivery. Expert Opinion on Drug Delivery, 3(6), 727-737.

[64] Işık, D., Joshi, A. A., Guo, X., Rancan, F., Klossek, A., Vogt, A., Rühl, E., Hedtrich, S., & Klinger, D. (2020). Sulfoxide-functionalized nanogels inspired by the skin penetration properties of DMSO. Biomaterials Science, 9, 712-725.

[65] Behzadi, S., Serpooshan, V., Tao, W., Hamaly, M. A., Alkawareek, M. Y., Dreaden, E. C., Brown, D., Alkilany, A. M., Farokhzad, O. C., & Mahmoudi, M. (2017). Cellular uptake of nanoparticles: journey inside the cell. Chemical Society Reviews, 46(14), 4218-4244.

[66] Salatin, S., & Yari Khosroushahi, A. (2017). Overviews on the cellular uptake mechanism of polysaccharide colloidal nanoparticles. Journal of Cellular and Molecular Medicine, 21(9), 1668-1686.

[67] Verdijk, P., van Veelen, P. A., de Ru, A. H., Hensbergen, P. J., Mizuno, K., Koerten, H. K., Koning, F., P. Tensen, C., & Mommaas, A. M. (2004). Morphological changes during dendritic cell maturation correlate with cofilin

activation and translocation to the cell membrane. European Journal of Immunology, 34(1), 156-164.

[68] Berges, C., Naujokat, C., Tinapp, S., Wieczorek, H., Höh, A., Sadeghi, M., Opelz, G., & Daniel, V. (2005). A cell line model for the differentiation of human dendritic cells. Biochemical and Biophysical Research Communications, 333(3), 896-907.

[69] Lechmann, M., Zinser, E., Golka, A., & Steinkasserer, A. (2002). Role of CD83 in the immunomodulation of dendritic cells. International Archives of Allergy and Immunology, 129(2), 113-118.

[70] Villadangos, J. A., Schnorrer, P., & Wilson, N. S. (2005). Control of MHC class II antigen presentation in dendritic cells: a balance between creative and destructive forces. Immunological Reviews, 207(1), 191-205.

[71] Grosche, L., Knippertz, I., König, C., Royzman, D., Wild, A. B., Zinser, E., Sticht, H., Muuler, Y. A., Steinkasserer, A., & Lechmann, M. (2020). The CD83 molecule–an important immune checkpoint. Frontiers in Immunology, 11.

[72] Lechmann, M., Berchtold, S., Steinkasserer, A., & Hauber, J. (2002). CD83 on dendritic cells: more than just a marker for maturation. Trends in Immunology, 23(6), 273-275.

[73] Li, Z., Ju, X., Silveira, P. A., Abadir, E., Hsu, W. H., Hart, D. N., & Clark, G. J. (2019). CD83: Activation marker for antigen presenting cells and its therapeutic potential. Frontiers in Immunology, 10, 1312.

[74] van Niel, G., Wubbolts, R., & Stoorvogel, W. (2008). Endosomal sorting of MHC class II determines antigen presentation by dendritic cells. Current Opinion in Cell Biology, 20(4), 437-444.

[75] Ju, X., Silveira, P. A., Hsu, W. H., Elgundi, Z., Alingcastre, R., Verma, N. D., Fromm, P. D., Hsu, J. L., Bryant, C., Li, Z., Kupresanin, F., Lo, T. H., Clarke, C., Lee, K., McGuire, H., Fazekas de St. Groth, B., Larsen, S. R., Gibson, J., Bradstock, K. F., Clark, G., J., & Hart, D. N. (2016). The analysis of CD83 expression on human immune cells identifies a unique CD83+-activated T cell population. The Journal of Immunology, 197(12), 4613-4625.

[76] Li, D., van Nostrum, C. F., Mastrobattista, E., Vermonden, T., & Hennink, W. E. (2017). Nanogels for intracellular delivery of biotherapeutics. Journal of Controlled Release, 259, 16-28.

[77] Zabihi, F., Koeppe, H., Achazi, K., Hedtrich, S., & Haag, R. (2019). One-pot synthesis of poly (glycerol-co-succinic acid) nanogels for dermal delivery. Biomacromolecules, 20(5), 1867-1875.

[78] Sonzogni, A. S., Yealland, G., Kar, M., Wedepohl, S., Gugliotta, L. M., Gonzalez, V. D., Hedtrich, S., Calderón, M., & Minari, R. J. (2018). Effect of

delivery platforms structure on the epidermal antigen transport for topical vaccination. Biomacromolecules, 19(12), 4607-4616.

[79] Frombach, J., Unbehauen, M., Kurniasih, I. N., Schumacher, F., Volz, P., Hadam, S., Rancan, F., Blume-Peytavi, U., Kleuser, B., Haag, R., Alexiev, U., & Vogt, A. (2019). Core-multishell nanocarriers enhance drug penetration and reach keratinocytes and antigen-presenting cells in intact human skin. Journal of Controlled Release, 299, 138-148.

[80] Edlich, A., Volz, P., Brodwolf, R., Unbehauen, M., Mundhenk, L., Gruber, A. D., Hedtrich, S., Hagg, R., Alexiev, U., & Kleuser, B. (2018). Crosstalk between core-multishell nanocarriers for cutaneous drug delivery and antigen-presenting cells of the skin. Biomaterials, 162, 60-70.

[81] Cobb, B. A., Wang, Q., Tzianabos, A. O., & Kasper, D. L. (2004). Polysaccharide processing and presentation by the MHCII pathway. Cell, 117(5), 677-687.

[82] Miller, M. A., & Pisani, E. (1999). The cost of unsafe injections. Bulletin of the World Health Organization, 77(10), 808.

[83] Bos, J. D., & Meinardi, M. M. (2000). The 500 Dalton rule for the skin penetration of chemical compounds and drugs. Experimental Dermatology: Viewpoint, 9(3), 165-169.

[84] Sykes, E. A., Dai, Q., Tsoi, K. M., Hwang, D. M., & Chan, W. C. (2014). Nanoparticle exposure in animals can be visualized in the skin and analysed via skin biopsy. Nature Communications, 5(1), 1-8.

[85] Eslami-Kaliji, F., Sarafbidabad, M., Rajadas, J., & Mohammadi, M. R. (2020). Dendritic Cells as Targets for Biomaterial-Based Immunomodulation. ACS Biomaterials Science & Engineering, 6(5), 2726-2739.

[86] Torkova, A. A., Lisitskaya, K. V., Filimonov, I. S., Glazunova, O. A., Kachalova, G. S., Golubev, V. N., & Fedorova, T. V. (2018). Physicochemical and functional properties of Cucurbita maxima pumpkin pectin and commercial citrus and apple pectins: A comparative evaluation. PloS One, 13(9), e0204261.

[87] Popov, S. V., & Ovodov, Y. S. (2013). Polypotency of the immunomodulatory effect of pectins. Biochemistry (Moscow), 78(7), 823-835.

[88] Kaplan, D. H. (2010). In vivo function of Langerhans cells and dermal dendritic cells. Trends in Immunology, 31(12), 446-451.

초 록

경피면역요법은 피부를 통해 항원을 전달할 수 있는 방법으로, 기존의 주사 면역 방식에 비해 상대적으로 비침습적이고 편리하다는 장점이 있다. 대사에 의한 분해를 우회하여 랑게르한스 세포 또는 진피 수지상세포를 표적으로 항원을 전달할 수 있다. 하지만 강하게 결합되어 있는 피부 층을 투과하는 것이 어렵기 때문에, 이를 극복하기 위해 감귤류 유래 펙틴을 사용하여 새로운 경피 항원 전달체로 쓰일 수 있는 나노젤을 개발하였다. 펙틴에 노보닌 그룹을 도입하여 펙틴 유도체를 합성하고 티올-엔 광클릭 반응을 통해 하이드로젤을 제조하였다. 이후 피부 투과가 가능한 것으로 알려진 100-300 nm 크기의 나노젤을 제조하기 위해 최적의 초음파 처리 공정을 확립하였으며, 초음파 처리 및 여과를 거쳐 균질한 크기 분포를 나타내도록 하였다. 해당 최적 공정을 거쳐 제조된 나노젤은 가교 밀도를 정밀하게 제어하여 오브알부민 담지 효율 및 분해성을 조절할 수 있었다. 또한 펙틴 나노젤은 돼지 피부의 각질층을 통과하여 표피와 진피까지 도달하였으며, THP-1 단핵구 파생 수지상세포에 함입되어 내부에 담지한 오브알부민을 전달할 수 있었다. 이후 HLA-DRA, CD80, CD83 과 같은 성숙화 관련 마커들의 발현량을 증가시켰다. 이와 같은 결과는 경피 항원 전달체로서 펙틴 나노젤이 우수한 성능을 나타낼 수 있다는 가능성을 보여준다.

주요어: 경피면역요법, 펙틴, 광클릭 반응, 나노젤, 수지상세포

학번: 2019-21536